Journal of Industrial and Engineering Chemistry 72 (2019) 31–49

Contents lists available at ScienceDirect

Journal of Industrial and Engineering Chemistry

journal homepage: www.elsevier.com/locate/jiec

Review

Recent advances in photoinduced catalysis for water splitting and environmental applications

Henry Agbe[a,1], Emmanuel Nyankson[b], Nadeem Raza[a,c,1], David Dodoo-Arhin[b], Aditya Chauhan[a], Gabriel Osei[b], Vasant Kumar[a], Ki-Hyun Kim[d,*]

[a] Department of Materials Science and Metallurgy, University of Cambridge, United Kingdom
[b] Department of Materials Science and Engineering, University of Ghana, Legon-Accra, Ghana
[c] Govt. Emerson College affiliated with Bahauddin Zakariya University, Multan, Pakistan
[d] Department of Civil and Environmental Engineering, Hanyang University, 222 Wangsimni-Ro, Seoul 04763, Republic of Korea

ARTICLE INFO

Article history:
Received 4 March 2018
Received in revised form 9 July 2018
Accepted 2 January 2019
Available online 9 January 2019

Keywords:
Photocatalysis
Light harvesting sensitizers
Oxygen evolving catalyst
Water reduction catalyst
Photo-anode
Band gap engineering

ABSTRACT

To secure reliable alternative energy sources, the up-conversion of solar energy into storable chemical energy holds promise. This review is organized to highlight recent advances in the fields of solar energy utilization and conversion methods with the aid of various heterogeneous catalysts. Special emphasis has been placed on TiO_2 photoanode catalysts, band-gap engineering, TiO_2-coupled light-harvesting molecules, and photon-coupled electron transfer via electron transport mediator systems. Furthermore, the coverage of this review extends to the topics of oxygen evolution catalysts, water reduction catalysts, and a system assembly capable of completing the four-electron water-oxidation reaction for efficient photocatalytic water splitting.
© 2019 The Korean Society of Industrial and Engineering Chemistry. Published by Elsevier B.V. All rights reserved.

Contents

* Corresponding author.
E-mail address: kkim61@hanyang.ac.kr (K.-H. Kim).
[1] These authors are considered as co-first authors because they contributed equally to this work.

https://doi.org/10.1016/j.jiec.2019.01.004
1226-086X/© 2019 The Korean Society of Industrial and Engineering Chemistry. Published by Elsevier B.V. All rights reserved.

Introduction

Although fossil fuels have been the main source of global energy, arguably due to their low cost, their significance is expected to diminish gradually and consistently for several reasons, including environmental concerns, perennial price fluctuations, and dwindling hydrocarbon reserves [1]. In contrast, the demand for renewable energy has been growing rapidly [2]. In the quest to meet global energy demand and secure environmentally benign energy sources, the development of renewable energy has become imperative.

Among various renewable sources, solar energy seems to be the most preferable option because of its abundance, low cost, and low carbon footprint. A quick analysis indicates that global energy demand could be met by harvesting 90 min of incident solar radiation [3]. Such a system could supply power at a rate of 1.2×10^5 TW ($1\,TW = 10^{12}$ J/s), which exceeds the current global power demand of 17 TW [3]. The primary challenge in harnessing solar energy lies in the high degree of uncertainty with regard to its availability, quality, and quantity. Incident solar energy is diffuse and sensitive to atmospheric and geographical conditions. One effective solution to this problem could be converting the solar energy into a form that can be used in the absence of natural sunlight.

A primary contender for solar energy storage is chemical up-conversion (H_2 production) through water splitting using artificial photosynthesis or the reduction of carbon compounds [4]. Another global problem that can be solved by harnessing solar energy is the mitigation of air and water pollution, which can be accomplished through photo-induced catalysis of pollutants. Photocatalysis can be defined as the mechanism through which a chemical transformation is accelerated by a catalyst with the aid of solar irradiation/light [5]. In theory, any semiconducting material able to harvest solar radiation and generate free radicals has photocatalytic potential. However, photocatalysis agents are generally large band-gap semiconductors, such as titanium dioxide (TiO_2), zinc oxide (ZnO), and cerium oxide (CeO_2). Low band-gap photocatalysts (e.g., cadmium sulfide (CdS) and iron oxide (Fe_2O_3)) do exist, but they have limitations (e.g., photo anodic corrosion) that limit their applications in many profitable fields (e.g., photocatalysts for water purification, water splitting, or oil spill remediation) [6]. Fig. 1 shows potential applications of photocatalysis. This review considers water splitting and environmental remediation, with particular focus on photocatalyzed water splitting. Figs. 2 and 3 show a simple flowchart for both processes.

TiO_2, or Titania, is one of the most studied large band gap semiconductors. It has long been regarded as the gold-standard against which to evaluate the performance of newer materials. Many reviews and published articles have detailed the benefits of using TiO_2 as the core photocatalyst in many applications [7,8]. Therefore, only a brief description will be provided here. Note that TiO_2 exists mainly in three phases of crystal structures (e.g., anatase, rutile, and brookite). Among those three, anatase and rutile are identified as the most common phases. The anatase phase of titania is preferred because of its excellent characteristics: it is photoactive, biologically and chemically inert, stable toward light (anodic corrosion free), inexpensive, and non-toxic [9]. The anatase phase is thus used as the most effective photocatalyst [7,10]. However, it absorbs selectively in the ultraviolet (UV) spectrum because of its high band gap (3.0–3.2 eV) [10,11]. The UV region constitutes only a minor fraction (3–5%) of the total solar energy relative to visible light (45%) and therefore cannot be used effectively for practical applications. In the early 1970s, the photocatalytic splitting of water on TiO_2 electrodes was first introduced by Fujishima and Honda [12]. Since then, researchers have shown great interest in TiO_2-based photocatalysts for renewable energy and environmental applications (organic pollutant degradation, disinfection of water, and production of hydrogen from water). Compared to standard chemical approaches, photocatalysis has the key advantage of using sunlight to activate and drive the degradation processes, making it more

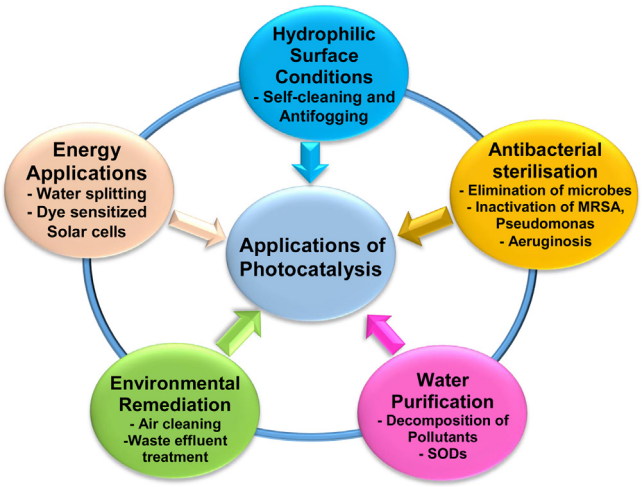

Fig. 1. Applications of photocatalysis.

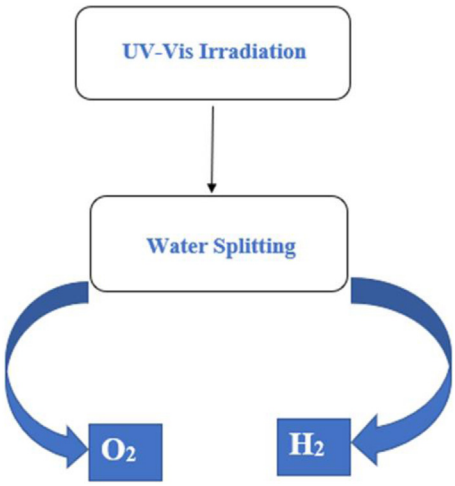

Fig. 2. Simple flowchart of water splitting.

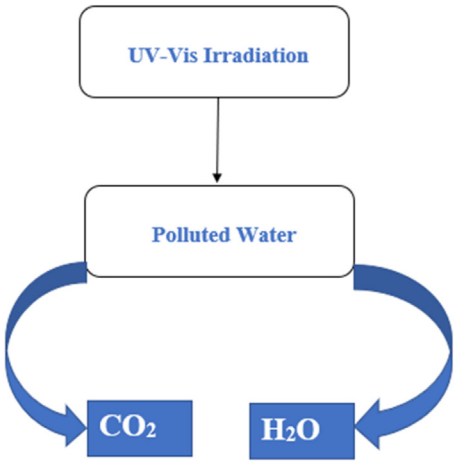

Fig. 3. Flowchart of mineralization of polluted water into carbon dioxide and water.

energetically sustainable and eco-compatible than other options. Nonetheless, several major challenges hinder the commercialization of photocatalytic technology, primarily the rapid recombination kinetics of photo-generated charge carriers and light absorption restricted to the UV region. To address those issues, a photocatalyst must be able to harness the visible spectrum (e.g., through metallic or non-metallic doping, a co-catalyst, or dye sensitization) and integrate various redox couples (akin to the proton-coupled electron transfer (PCET) process in natural photosynthesis).

In a typical photosynthesis process, light absorption by chlorophyll and other accessory pigments (chlorophyll b and beta-carotene) excites electrons to initiate a series of redox reactions similar to the electron transfer chain reaction in mitochondria. Photo-excited electrons are transferred from water at the reaction center (photosystem II, specifically at the manganese-containing oxygen evolving complex (OEC)) to a higher energetic state (oxidized primary electron-donor chlorophyll (P680*)). The P680* subsequently decays as electrons transfer to the primary and secondary quinone cofactors Q_A (primary plastoquinone electron acceptor) and Q_B (secondary plastoquinone electron acceptor) and eventually to photosystem I [13]. The abstraction of electrons from water by P680 breaks the water into its ionic components (H^+ ions and O^{-2} ions). The O^{-2} ions combine to form diatomic O_2, which is released when the protons are pumped from the tyrosine phenolic group to a nearby histidine group using electron potential gradients. Thus, this charge separation process prevents recombination. For successful water oxidation, however, the redox potential of the tyrosine must be located between that of P680* and that of the OEC [13]. At photosystem I (P700), photo absorption excites electrons to a higher energy state to begin another series of redox reactions that form the energy carrier molecule (NADPH) needed for the subsequent light-independent carbon fixing process.

An analysis of recent literature on photocatalytic water spitting approaches indicates that most efforts have been directed intensively toward the design of optimal photoanode material [14,15]. However, the design of metal-free photocatalysts (e.g., carbon nitride, boron carbon nitride, covalent organic frameworks, and black phosphorus) for water splitting and environmental applications (details in subsequent section) is also gaining interests of scientific community in recent times [16–22].

Although some excellent reviews on artificial photosynthesis have been made over the last 30 years [23–30], compact system assembly (with an emphasis on photoanode material coordinated with a photosensitizer and catalyst) has been scantily reported. A detailed review on complete designs for compact system assembly is very desirable because the complete system could transfer four oxidizing equivalents to generate oxygen gas and hydrogen gas. Furthermore, the charge separation processes of photosystems I and II are known to provide 100% quantum efficiency under optimal conditions [31]. Consequently, it is desirable to apply biomimicking of the PCET processes to design an artificial water splitting system with improved quantum efficiency.

This review discusses the basic features and mechanisms of TiO_2 photo anode catalysts, along with advances in band-gap engineering and light-harvesting molecules coupled to semiconductor surfaces. It also provides a detailed report of PCET via an electron transport mediator system akin to the electron transfer process in all photosynthetic organisms (plants, cyanobacteria, etc.). Shortcomings in the current literature are also briefly discussed, along with the provision of future directions for water splitting technology. Finally, OECs and a complete system assembly that can complete the four-electron water-oxidation reaction are discussed to help develop an efficient photocatalytic water splitting system.

Photoanode materials

Many semiconductors are used as anode materials for photocatalysis and photo-electrochemical applications. These generally include metal oxides, metal nitrides, metal sulfides, and metal-free catalysts.

Metal oxides

Materials for photo anodes, particularly metal oxides, generally suffer from both surface and bulk electron–hole recombination. However, this shortcoming can be largely resolved through the adoption of nanoscale phases [32]. Different nanostructures have been synthesized with various 1D (nanotubes, nanorods, nanowires, nanobelts, and nanoneedles) [33], 2D (nanowells) [34], and 0D (nanodots) [35] morphologies to achieve excellent conductive scaffolds for photo-electrochemical water splitting, along with the overall photocatalytic degradation of pollutants. Metal oxide photo anodes are the most widely used photocatalysts for both photocatalysis and photo-electrochemical applications [36]. Metal oxides commonly selected by researchers include TiO_2, Fe_2O_3, WO_3, ZnO, Cu_2O, Al_2O_3, Ga_2O_3, Ta_2O_5, CoO, and ZrO_2 [36,37]. An ideal metal oxide photocatalyst must be stable (no anodic photo corrosion at the semiconductor–electrolyte interface), non-toxic, inexpensive, and readily available, while offering reasonably high quantum efficiency [38]. To date, various metal oxides have been researched extensively, and TiO_2 seems to be the material that best fulfills these conditions [9]. Consequently, it is the main photo anode considered in this review (Fig. 4).

Charge carrier interface dynamics

Charge carrier interface dynamics take different forms, as shown in Fig. 5. For example, the semiconductor can donate electrons to acceptors to reduce the acceptor (pathway (1)), while holes migrate onto the surface to oxidize the donor species (pathway 2). Additionally, if the recombination of the generated electron–hole pairs takes place, the input energy can be dissipated in the form of heat (surface recombination) or emitted light (pathway (3)). The carriers can also recombine within the bulk of the photocatalyst through a volume recombination pathway (4). Because these recombination processes can reduce the overall efficiency of a photocatalytic process, it is ideal to adopt a nanostructured photocatalyst that increases efficiency by suppressing volume recombination.

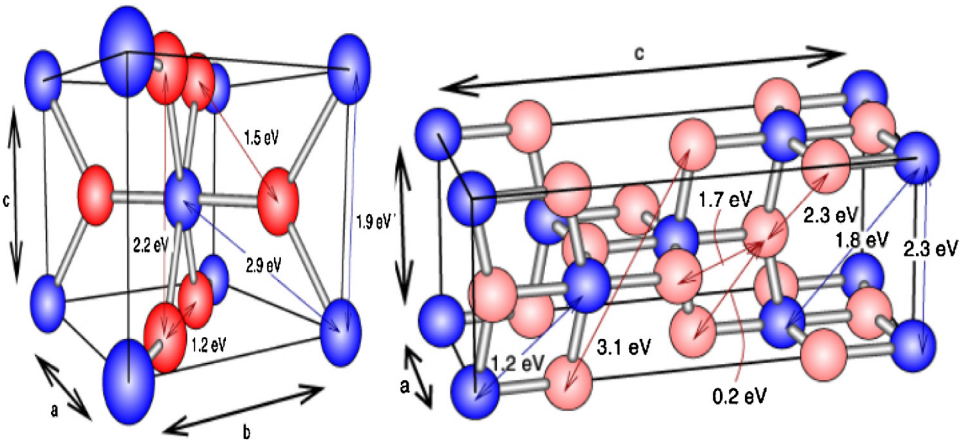

Fig. 4. Lattice structures of (a) rutile and (b) anatase TiO_2 [269].

For photocatalytic degradation of pollutants, the reaction mechanism generally follows the following schemes [39]:

$$TiO_2 + hydrocarbon(h\nu) \rightarrow CO_2 + H_2O \quad (1.1)$$

$$TiO_2 \rightarrow TiO_2(e^- + h^+) \quad (1.2)$$

$$O_{2(ads)+e^-} \rightarrow \cdot O_2^- \quad (1.3)$$

$$\cdot O_2^- + H_2O \rightarrow HO_2 \cdot + OH^- \quad (1.4)$$

$$2HO_2 \cdot \rightarrow H_2O_2 + O_2 \quad (1.5)$$

$$H_2O_2 + h\nu \rightarrow 2 \cdot OH \quad (1.6)$$

$$OH^- + h^+ \rightarrow \cdot OH \quad (1.7)$$

Water splitting electron–hole dynamics follow similar schemes. Consider that the absorption of an incident photon that has energy greater than the band gap of the photocatalyst ($\lambda < 390$ nm) takes place. Then, electrons in the valence band (VB) edge are excited into the base of the conduction band (CB) to leave a hole in the VB. Accordingly, water molecules are reduced by the electrons to form H_2 and are oxidized by the holes to form O_2 for overall water splitting, as displayed in Fig. 6. Details are given in "Complete system assembly" [14].

To achieve a desirable electron transfer, the negative potential of the electron acceptor species should be below the CB of the semiconductor (more positive than the semiconductor). Similarly, the positive potential of the electron donor species should be above the VB of the semiconductor (more negative than the semiconductor). The photocatalyst must be able to oxidize the donor species. Two reference energy levels that acquire particular relevance with respect to most photocatalytic processes can be considered references: the reduction of protons (E NHE (H^+/H_2) = 0.0 eV) and the oxidation of water (potential of normal hydrogen electrode E, NHE (O_2/H_2O) = 1.23 eV) [40].

In general, metal oxide semiconductors have a VB with a main contribution from oxygen 2p orbitals located 1 to 3 eV below the O_2/H_2O redox couple [40]. Their CBs constitute transition metal cations of d^0 and d^{10} orbital configurations. The CB position is close to, or lower than, the H_2O reduction potential (Fig. 7). Note that wide band gap materials are effective photo oxidation catalysts, although they absorb mostly in the UV region of the electromagnetic spectrum [40]. In contrast, the VBs of metal sulfide and metal nitride photocatalysts are usually composed of (S) 3p and (N) 2p orbitals, respectively [14]. The band edges of the metal sulfides are usually situated within or close to both the reduction and oxidation potential of H_2O. In other words, both the oxidizing (VB holes) and reducing power (CB electrons) are lower than those of non-transition metals [40]. Therefore, they have narrower band gaps for visible light absorption (500–600 nm) than metal oxides [14]. However, they are unsuitable for splitting water into H_2 and O_2 without proton donors/sacrificial reagents [14]. Recently, metal sulfides and nitride have been applied in photo-electrochemical cells, although metal sulfides such as CdS cannot produce O_2 because of photo corrosion [15,41,42]. Photo corrosion occurs when the S^{2-} in cadmium sulfide becomes oxidized by a hole instead of water molecules through the following reaction:

$$CdS + h^+ \rightarrow Cd^+ + S \quad (1.9)$$

Band gap engineering

As noted above, a major problem in the practical application of photocatalysts is rapid electron–hole carrier recombination and UV absorption. To overcome this challenge, several strategies have been adopted to either modify the band gap of the photocatalysts or extend the absorption spectrum of the photocatalysts into the visible region of the electromagnetic spectrum, including non-metal [43–45] and metal [42,46–50] doping, dye sensitization [51–54], and semiconductor coupling [51,55].

Non-metal doping

Non-metal doping of metal oxides is a recent strategy that has generated interest in visible-light-active photocatalysis because it is more efficient than most metallic doping through a decrease in recombination centers. A variety of non-metal anions (N, S, C, F, etc.) have been implemented to enhance the visible-light photocatalytic activities of metal oxides, particularly TiO_2. Among these anions, nitrogen-doped TiO_2 has received a lot of attention because its atomic size is similar to that of oxygen, and its high stability achieves a low ionization potential [56–60] and enhanced visible light absorption. Note that substitutional doping of C, N, F, P, and S for O in anatase TiO_2 was first introduced by Asahi and co-workers [43]. Since then, various research groups have designed visible-light-active N-doped TiO_2 photocatalysts [61–63]. As the 2p states

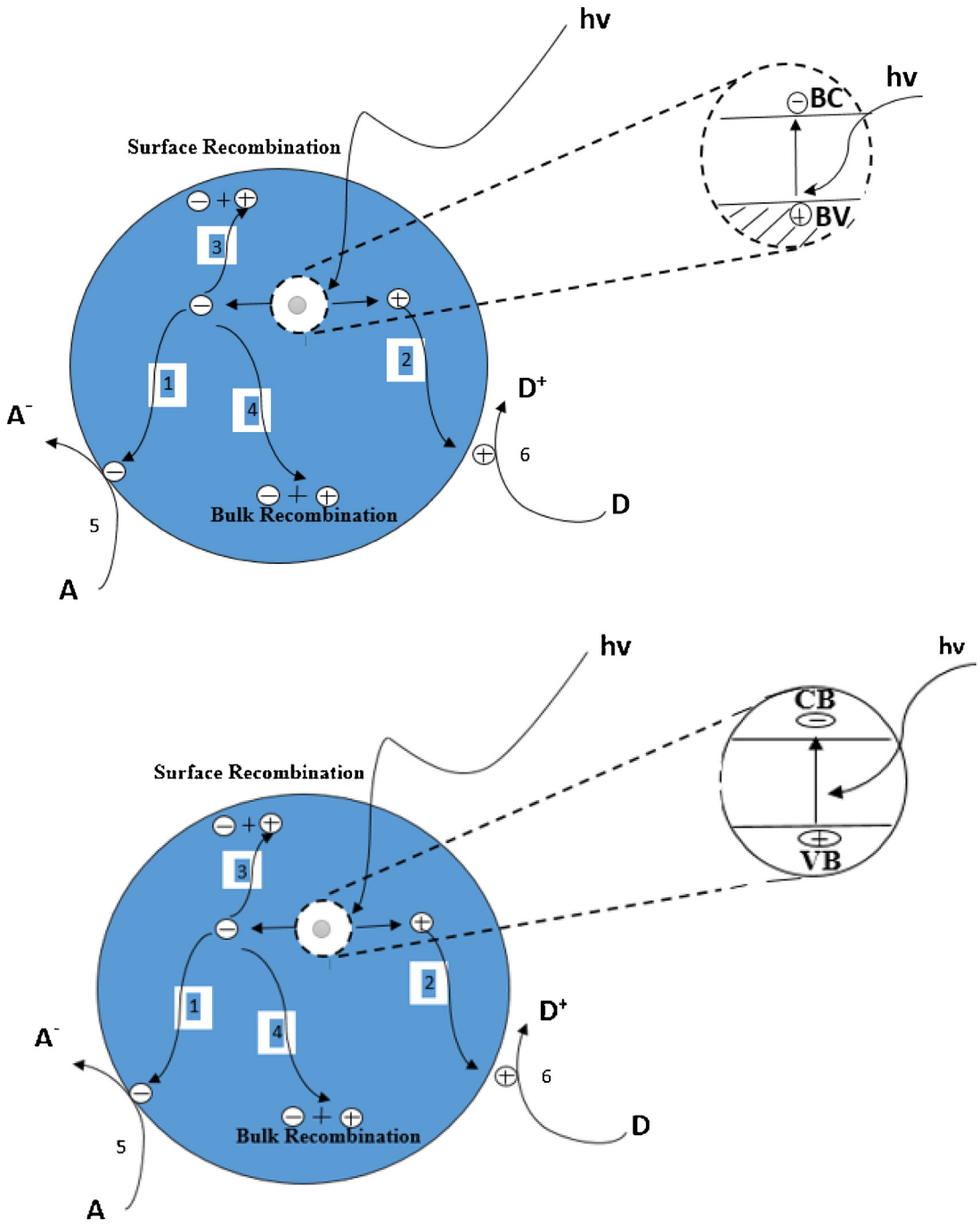

Fig. 5. Schematic showing charge carrier dynamics upon irradiation of a semiconductor: 1 electron transport to the surface, 2 hole transport to the surface, 3 surface recombination, 4 bulk recombination, 5 electron transference to an acceptor molecule, and 6 hole trapping by a donor molecule (adapted from [40]).

of N are mixed with those of O, it could shift the VB edge upward to narrow the band gap of TiO_2 [43].

The band gap narrowing of the energy levels of the VB and CB was controlled by several variables, including the dopant concentration level and strong interactions among the impurity energy states, VB, and CB [56]. However, predictions based on the density functional theory indicate that doped N atoms can occupy substitutional or interstitial sites in the TiO_2 lattice to generate localized energy levels in the band gap [64]. For dopants occupying substitutional positions, a continuum of slightly higher energy levels essentially extends the VB, whereas an interstitial dopant results in discrete energy levels above the VB, often called a mid-gap state (Fig. 8) [65]. The visible light response in the doped photocatalyst arises from the electron transition from localized N orbitals to the CB or surface-adsorbed O_2 [64].

For visible-light-active photocatalysis, sulfur can be used as a non-metal dopant instead of nitrogen. Sulfur doping has been performed in the forms of hexavalent (S^{6+}), tetravalent (S^{4+}), and sulfide (S^{2-}), depending on the synthetic method adopted for S-doping of TiO_2 [66,67]. S-doping results in band gap narrowing similar to that with nitrogen, but it is difficult to incorporate S into the TiO_2 crystal structure because of its large ionic radius relative to oxygen. C and P, on the other hand, are less effective because their mid-gap states penetrate deep into the TiO_2 crystal, which traps the photo-generated charge carriers and renders them unable to migrate to the active sites to undergo a redox reaction with the

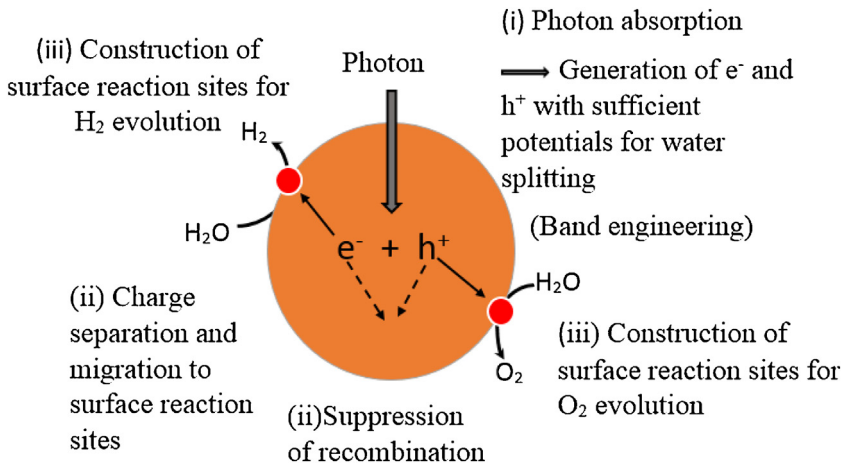

Fig. 6. Main processes in photocatalytic water splitting [14].

adsorbates [68]. Non-metal doped photocatalysts are synthesized mainly by physical and chemical methods, such as reactive DC magnetron sputtering, sol–gel, hydrothermal, and solvothermal methods.

Noble metal loading

The use of noble metals (e.g., Pt, Au, Pd, Rh, Ni, Cu, and Ag) can effectively improve the efficiency of photocatalysis [69–74]. Primarily, as the noble metals act as an electron sink, the photo-generated electrons can be suppressed to recombine with the hole. Other benefits include Schottky junction formation and localized surface plasmon resonance. Because their fermi levels are lower than that of TiO_2, photo-generated electrons can be transferred from the CB to metal particles coupled to the surface of the photocatalyst for enhanced electron–hole charge separation.

To investigate the electron transfer dynamics between the CB and metal particles, electron spin resonance spectroscopy is a useful tool. Electron transfer between Pt nanoparticles and TiO_2 was assessed by electron paramagnetic resonance spectroscopy [69]. Accordingly, as irradiation time increased, Ti^{3+} signals increased proportionately. Again, Pt loading reduced the amount of Ti^{3+}, indicating the occurrence of electron transfer. The accumulation of electrons on the metal particles lowers their fermi levels and shifts them more toward the CB of the TiO_2, thereby making the CB more negative [75]. This is beneficial for both water splitting and environmental applications. In the former, the transferred electrons can reduce the protons and enhance hydrogen production. In the latter, molecular oxygen can be reduced to superoxide radicals and their concomitant radicals for efficient photodegradation of pollutants.

Various studies have investigated methods for the synthesis of doped titania and the effects of noble metal-modified TiO_2 on hydrogen production [47]. Bamwenda et al. investigated the effects of Au and Pt nanoparticles on the photocatalytic activity of TiO_2 materials through the photocatalytic splitting of a water–ethanol

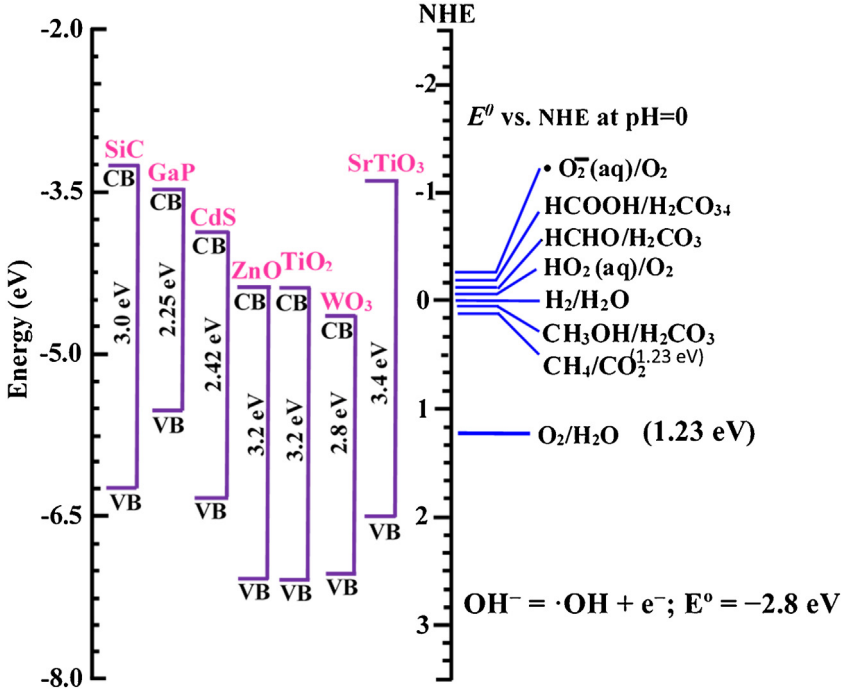

Fig. 7. Relationship between band structure of a semiconductor and its redox potential for water splitting [40].

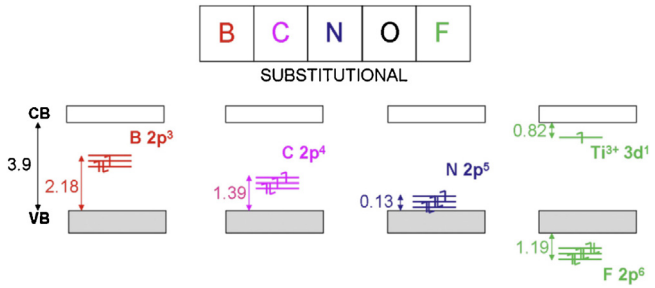

Fig. 8. Schematic of B-C-N and F doping of TiO_2 [64].

mixture [76]. They found that Pt loading worked better than Au loading, and that Pt-loaded TiO_2 was less sensitive to that method of synthesis than Au-loaded TiO_2. Therefore, they concluded that optimal loading was important because loading above the optimal level resulted in a reduction in photo absorption by TiO_2, probably because of electron–hole recombination centers [47]. Again, Pt and Au loadings were more effective than Pd loading because of their suitable electron affinity and work functions [47]. One drawback of metal doping, particularly transition metals, is their tendency for electron–hole recombination.

Metals have also been used to increase absorption in the visible region through plasmon resonance of the photocatalyst. The collective oscillation of conducting electrons in the metal nanoparticles can sensitize TiO_2 nanoparticles. Plasmonic resonance in the visible spectral range has been observed in Ag [77,78] and Au [47,79]. Ag nanoparticles act as efficient antennae for capturing solar energy (Fig. 9). Modifying semiconductor nanostructures with plasmonic metal-nanoparticles improved their efficiency in various applications, including water splitting, decomposition of organic compounds, and photovoltaic devices (by 10–15%) [80–84].

Semiconductor coupling

Coupling semiconductors for visible-light-active photocatalysis has been investigated by several research groups [51,85–87]. Large band gap semiconductors such as TiO_2, ZnO, and SnO_2 can be coupled to low band gap semiconductors (CdS) to improve photocatalysis efficiency. Specifically, TiO_2 has been coupled with CdS for improved efficiency relative to either TiO_2 or CdS alone [86,87]. To do that, one of the semiconductors must have a more negative CB level than the other. Thus, the CB level of the smaller band gap material must be more negative than that of the wide band gap material. Consequently, CB electrons can be injected from

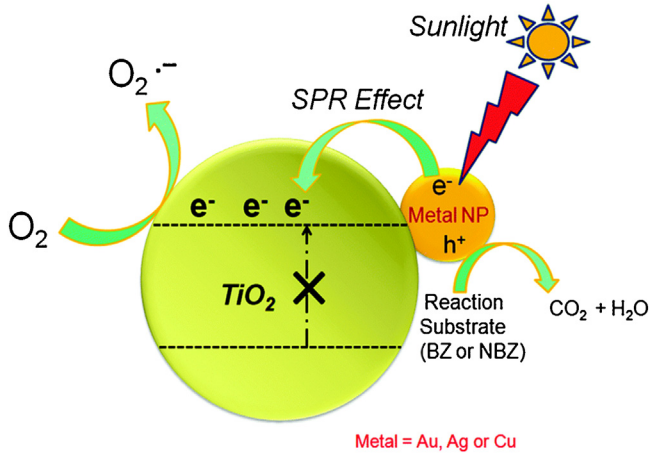

Fig. 9. Surface plasmon resonance effect of metal-doped TiO_2 [270].

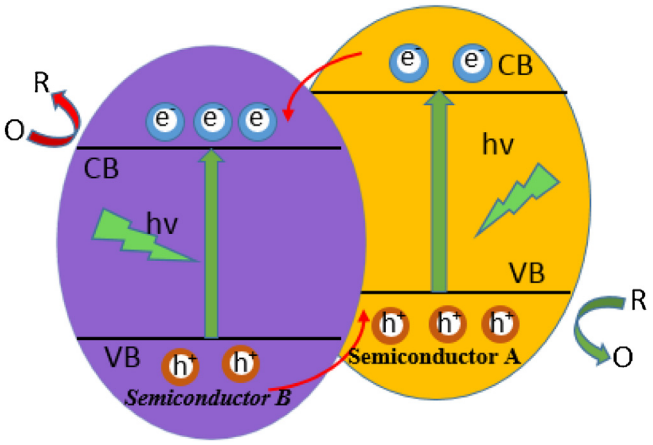

Fig. 10. Semiconductor coupling (adapted from [271]).

the small band gap semiconductor to the large band gap semiconductor (Fig. 10). Thus, wide electron hole separation can be achieved. However, if the hole is not scavenged, S^{-2} from the CdS can be attacked, which results in photo corrosion. In the presence of sacrificial agents (such as ethylene diamine tetra-acetic acid (EDTA) or tri ethanol amine), photo corrosion can be prevented. Thus, a synergetic effect between the visible-light-active property of CdS and the photostability of TiO_2 improves photocatalysis efficiency.

Coupling heterogeneous semiconductors for visible-light-induced water splitting and environmental remediation has also been investigated [88,89]. Specifically, when TiO_2 (band gap 3.2 eV) was coupled with CdS (band gap 2.4 eV) and SnO_2 (band gap 3.5 eV), the small band gap CdS (CB = −0.76 eV) caused visible-light sensitization to transfer electrons from the TiO_2 into the CB of the SnO_2 (CB = −0.34 eV) [51,90], which resulted in efficient electron–hole separation and enhanced water splitting photocatalytic activity. Similar work (photoexciting both semiconductors) was done by Doong et al. to investigate semiconductor coupling for environmental applications [85]. Specifically, CdS was coupled with TiO_2 for 2-chlorophenol degradation under UV irradiation [85]. The synergic effect of the two semiconductors produced better photocatalytic activity through better charge separation. Thus, CB electrons for CdS were injected into the CB of TiO_2 while corresponding VB holes for TiO_2 impinged on the VB of CdS.

Dye sensitization

Similar to heterogeneous semiconductor coupling, chemical chromophores can be used as an antenna for harvesting light-like pigments in algae and higher green plants. Dye sensitization is one of the most effective ways of extending the photo response of TiO_2 into the visible region [51–54,91–94]. Dye sensitization is advantageous because it enables absorption in the visible and near infrared regions and accelerates the injection of electrons to the semiconductor; it can also be grafted onto a host surface by surface links and anchoring molecules. These types of reactions are exploited in dye sensitized solar cells [95].

In dye sensitization, the CB of the semiconductor acts as a mediator for electron transfer rather than as a conventional photocatalyst. Some dyes, such as safranine O/EDTA and T/EDTA, absorb visible light and produce electrons as reducing agents for hydrogen production [96]. However, without an appropriate mechanism to efficiently separate the photo-generated excitons, the rate of hydrogen production by the dyes is rather low because of electron–hole recombination [68]. A typical mechanism for dye-sensitized semiconductor photocatalyst water-splitting involves

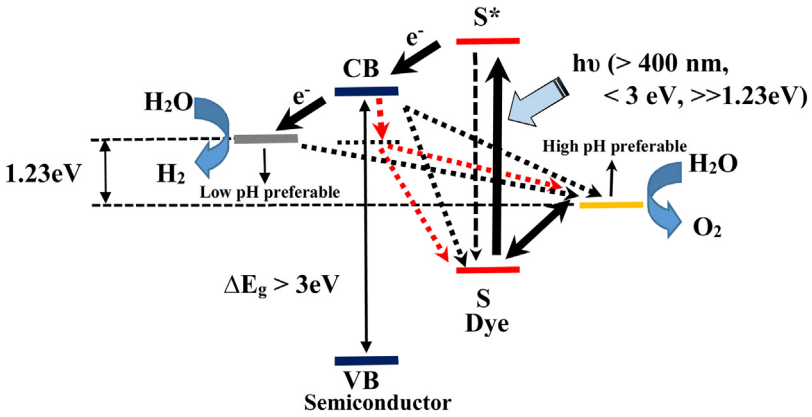

Fig. 11. Proposed mechanism of dye-sensitized photocatalysis under visible light irradiation including forward electron transfer and possible recombination pathways [40].

visible light illumination followed by electron injection from the excited dyes into the CB of the semiconductors to initiate the catalytic reactions, as illustrated in Fig. 11.

For efficient visible-light absorption and electron transfer, the forward electron transfer rate must be faster than the sum of all the reverse rates in the same system [40]. It has been reported that the forward reaction occurs on a femtosecond scale, whereas the rate of recombination occurs on a nanosecond to millisecond scale [97–100]. One major disadvantage of using dye-sensitization with semiconductors is their tendency to self-degradation under prolonged solar irradiation. Using appropriate sacrificial agents or redox systems, such as EDTA and I_3^-/I^- pairs, to regenerate the dye can address that issue [101]. Applying photocatalysis for water splitting, water purification, and environmental remediation has been investigated intensively using different dyes (Table 1). Regardless of the practical application, dye sensitizers have to meet several common requirements (details in Section "Photoanode materials") [40]. In addition, an efficient light harvesting chromophore must fulfil other conditions, such as the ability to bind to anchoring groups, an optimal number of anchoring groups, stable linkages, and the polarity of the suspending solvent [40]. Details are given in Section "Anchoring groups for photosensitizers and catalysts". All these factors need to be considered to design a highly efficient light harvesting chromophore system able to absorb a wide spectral bandwidth of sunlight for photocatalysis applications.

The design of metal-free photocatalysts

Recently, a new class of metal-free photocatalysts (B, S, P) including binary carbon nitride, boron carbide, polymeric g-carbon nitride (g-C3N4), hexagonal-ternary boron-carbon-nitride (BCN -integrated with Cobalt), and black phosphorous nanosheets [16–22] have emerged. Many of them have actually become important as efficient photocatalysts for both water splitting and environmental remediation. Metal-free photocatalysts are less costly alternative to conventional metal-based photocatalyst with the minimal negative environmental impact; this is at least partially because they do not leach out metal ion as metal-based photocatalysts do [102]. Polymeric g-C_3N_4 photocatalyst, in particular, has several advantages as water splitting medium, photocatalyst, and CO_2 convertor. For example, this metal-free photocatalyst is a visible-light-response material (2.7 eV bandgap) [103]. Therefore, it is highly ideal for practical application, as g-C_3N_4 has effective charge/electron pathway, better stability, and larger active specific surface areas [104,105]. Additionally, the photocatalyst can easily be synthesized using cheap N-rich precursors (dicyanamide, cyanamide, melamine, and urea) and sol–gel methods [103,106,107]. Consequently, g-C_3N_4 photocatalysts have become highly preferable option in recent time. For example, Wang et al. prepared a novel g-C_3N_4 by thiocyanuric acid self-polymerization in N_2 atmosphere [108]. The obtained g-C_3N_4 had excellent water oxidation ability compared to commonly used photocatalysts (TiO_2) [102]. Again, a modified metal-free photocatalyst (WS_2/g-C_3N_4), synthesized via ultrasound-assisted hydrothermal method, was recently demonstrated to exhibit high excellent photoactivity [19]. The photocatalyst had the ability to regenerate NAD+ to NADH. Furthermore, the photocatalyst was able to convert CO_2 to methanol under visible light irradiation. This multifunctional photocatalyst was highly useful for CO_2 conversion along with enhanced photodegradation capability against

Table 1
A list of sensitized photocatalysts used in (A) water splitting and (B) photocatalytic degradation reactions under visible light irradiation.

Order	Sensitizer	Catalyst	Hydrogen evolution (μmol/h)	Apparent quantum efficiency (%)	Refs.
A: Water splitting					
1	Eosin Y	Pt/TiO_2	65	10	[10]
2	Eosin Y	Rh/TiO_2	14.63	7.10	[214]
3	Eosin Y	CuO/TiO_2	10.56	5.1	[215]
4	Eosin Y	Pt/MWCNT	54.20	12.14	[216]
5	Eosin Y	Pt/Ti-MCM-41	10	12.01	[217]
6	Eosin Y-Fe^{3+}	Pt/TiO_2	275	19.1	[218]
7	Ru complex	Pt/TiO_2	Max. 132	22.4	[219]
B: Photocatalytic degradation					
			Target contaminant	Degradation efficiency	
8	Ru complex	TiO_2	Herbicide terbutryn	100% (4 h)	[220]
9	Ru complex	TiO_2	CCl_4	0.4461 M min^{-1} g^{-1}	[221]
10	Ru complex	TiO_2	CCl_4	0.5851 M min^{-1} g^{-1}	[222]
11	Polyaniline	TiO_2	Methylene blue	80% (1.5 h)	[223]
12	Poly(fluorene-co-thiophene)	TiO_2	Phenol	74.3% (10 h)	[224]

Rhodamin B dye. 100% RhB degradation was achieved less than 1 h of UV–vis irradiation. Futher, the photocatalysts was still stable even after five runs of photocatalysis.

The enhanced potential of hexagonal boron carbon nitride (*h*-BCN) semiconductor has also been noted in recent times as efficient metal-free photocatalysts. Note that both graphene and h-BN have undesirable band gaps of 0.0 eV and 5.5 eV, respectively. However, it has been reported that the intermediate layered materials (called the ternary boron carbon nitride (B-C-N) compounds) can constitute the desired medium-bandgap semiconductors where bandgap and absolute energy levels can be adjusted by chemical variations [109,110]. For instance, Lu et al. [110] synthesized a ternary B-C-N semiconductor that could be used for catalysis of hydrogen or oxygen evolution from water as well as carbon dioxide reduction under visible light illumination. The ternary B–C–N alloy featured a delocalized two-dimensional electron system with sp_2 carbon that was incorporated into the h-BN lattice. The bandgap could be adjusted by the amount of incorporated carbon to produce unique functions. Again, in a related work, Zhang et al. [111] integrated hexagonal boron carbon nitride (*h*-BCN) semiconductor cobalt ions to catalyze oxygen evolution reaction (OER) with light illumination, without using noble metals. Again, in this study, the high efficiency of the oxygen evolution was also attributed to the synergistic effect between the cobalt ions and the large specific surface area of the *h*-BCN.

Another emerging metal-free photocatalyst worthy of mentioning is two-dimensional material, black phosphorus (BP) nanosheet. BP nanosheet is important because it has unique chemical and physical properties such as: high carrier mobility, tuneable optical absorption, and novel electronic band structure [112]. Wang et al. [21] demonstrated the influence of many-body effects of BP nanosheet on photocatalytic efficiency and proved that the ultrathin BP nanosheets were excitation-energy dependent with optical switch ability effect on photocatalytic generation of reactive oxygen species (ROS). Such photocatalysts with both photo-excitation and ROS dependence can be beneficial for solving practically for wastewater and environmental problems.

Overall, new emerging metal-free photocatalysts can help in providing solutions to current challenge (e.g., light absorption limitations) associated with both metal oxides and metals photocatalysts. The inability to absorb in the visible region of the electromagnetic radiation has hindered the use of photocatalyst to solve global water and energy crises. It is desired that the use of metal-free photocatalysts alone or coupled with existing metal and metal oxide based photocatalysts could hopefully help solve the global energy and environmental problems. Table 2 below shows timeline for key developments in overall water splitting photocatalysis since 1972.

Light-harvesting photosensitizers

As noted above, a photosensitizer acts as an antenna for absorbing photons in the visible and near infrared regions of the solar spectrum. An ideal photosensitizer meets a list of requirements, such as the potential to absorb across a wide range of wavelengths in the visible and near infrared regions, the ability to convert all absorbed photons into electron–hole pairs, being both photo and redox stable, having a suitable anchoring group bound to the photo anode surface, and having the appropriate redox potential to drive the catalytic oxidation of water in a water oxidation catalyst (WOC) [3,113]. Obviously, most dyes cannot meet these stringent requirements. Common dyes that have gained interest for sensitizing photocatalysts, particularly TiO_2, include metal complexes [114,115], porphyrins [116], and organic dyes [117].

Ruthenium-polypyridyl sensitizers

Ruthenium (II) tris bipyridine has been extensively applied as an efficient photo anode sensitizer for the production of hydrogen and oxygen [3,118–122] because of its unique characteristics, such as broad coverage and high molar absorptivity in the visible region. It exhibits strong absorptivity below 500 nm (molar extinction coefficient at 450 nm = 14400 M^{-1} cm^{-1}), good redox potential, a long excited-state lifetime (600 ns), and good electrochemical stability, and its spectroscopic and electrochemical properties can be tuned to optimize performance [3]. In coordination compounds such as $[Ru(bpy)_3]^{2+}$ derivatives, major visible absorption occurs in the metal-to-ligand charge transfer (MLCT) band, with an absorbance maximum of 450–470 nm (454 nm = 2.7 eV) [113]. As light is absorbed, electrons are promoted from the metal d-orbitals of the Ru^{2+} to the conjugated bipyridine ligands, $d(p) \rightarrow p*$ [123,124], to form a singlet state with a life period of 100–300 fs. Transient absorption spectroscopy shows that, within a period of 100–300 fs, the singlet undergoes intersystem crossing to form triplet MLCT states [125]. In contrast, the lifetime of the triplet state is relatively long (600 ns) because relaxation to the ground state is spin-forbidden, particularly for $[Ru(bpy)_3]^{2+}$ and many of its derivatives (Fig. 12) [115]. Because $[Ru\ (bpy)\ _3]^{2+}$ is a $d\pi^6$ coordination compound, its optical properties (such as color) can be tuned by synthetic chemistry. For example, the MLCT absorption bands can be tuned in energy by altering the

Table 2
Timeline of key developments in overall water splitting photocatalysis technique.

Time line	Discovery	Type
1972	Discovery of photochemistry water splitting [12]	Other
1979	Proposal of Z scheme Model [225]	OWS* via two-step Photoexcitation
1980	OWS on Particulate Photocatalysts [226,227]	OWS via one-step Photoexcitation
1982	New Oxide Photocatalysts with layered and tunnelled structures [228,229]	OWS via one-step Photoexcitation
1998	New Oxide Photocatalysts via control of valence Band maximum [230,231]	Other
2001	D^{10} as new photocatalyst group e.g. $ZnGa_2O_4$ [232–234]/Z-Scheme OWS with aqueous redox mediator [234–236]	OWS via one-step Photoexcitation/OWS via one-step Photoexcitation
2002	Non-Oxide as new Photocatalysts (oxy-sulphide and oxy-nitrides) [237–240]	Other
2005	OWS on d^{10} oxy-nitrides (Ge_3N_4 and GaN:ZnO) [240,241]	OWS via one-step Photoexcitation
2009	Z-Scheme OWS via solid state charge transfer ($SrTiO_3$: Rh + $BiVO_3$) [242]	OWS via two-step Photoexcitation
2013	OWS on d^{10} Oxy-nitrides (ZrO_2/TaON: <520 nm) [243]	OWS via one-step Photoexcitation
2014	Natural-Artificial Hybrid Z-Scheme OWS system [244]/OWS on Metal-doped Oxide ($SrTiO_3$: Rh, Sb; < 520 nm) [245]	OWS via two-step Photoexcitation/OWS via one-step Photoexcitation
2015	OWS on 600 nm class d^{10} oxy-nitrides ($LaMg_xTa_{x-1}O_{1+3x}N_{2-3x}$) [246,247]	OWS via one-step Photoexcitation
2016	OWS on Metal free-semiconductor of C_3N_4 (<442 nm) [248]	OWS via one-step Photoexcitation

OWS* = Over all water splitting.

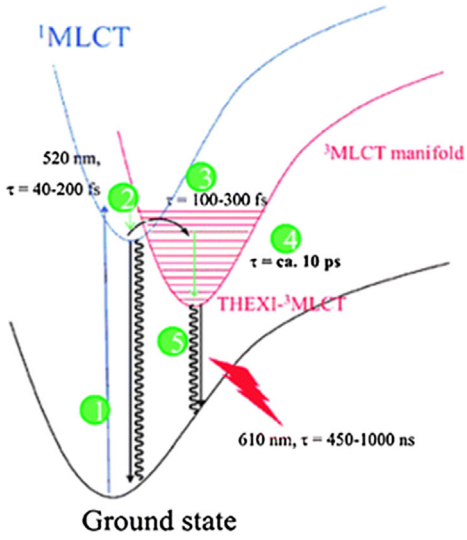

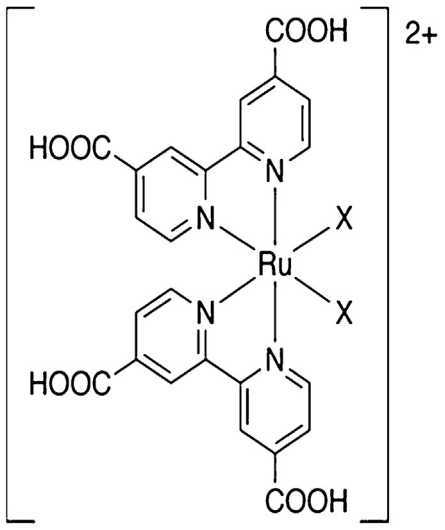

Fig. 12. Lennard–Jones potential energy wells illustrating the relative electronic and vibrational energies and lifetimes of Ru $(bpy)_3^{2+}$ (1). Both internal-conversion thermal relaxation (2) and intersystem crossing (3) occur on the sub-picosecond timescale, whereas the lifetime of the their state (4) is up to a microsecond (left) [115]. Ruthenium-polypyridyl complex reported by Grätzel and co-workers, where X = Cl, Br, I, CN, or SCN (right).

substituents on the polypyridyl complex (bpy) ligands or controlling the extent of d(p)-p* back-bonding donation to non-chromophoric ligands [115]. This enables a red shift and absorption in the visible and infrared regions. Grätzel et al. reported that ruthenium complexes in the form of $[Ru(4,4\text{-}(COOH)_2bpy)_2(X)_2]^{2+}$, where X = Cl, Br, I, CN, or SCN, were excellent photosensitizers for TiO_2.[3] In particular, the thiocyanato complex $(NBu_4)_2[Ru(4,4\text{-}(COOH)(COO)bpy)_2(NCS)_2]$, also called N719 or red dye, exhibited an extinction coefficient of ~14,000 $M^{-1}\,cm^{-1}$ at 534 nm and an incident photon-to-current conversion efficiency exceeding 80% between 480 and 600 nm [126].

Porphyrin sensitizers

Porphyrin and macrocyclic chromophores have been studied as sensitizers for water splitting reactions [127–129] and dye sensitized solar cells (DSSCs) [130–132]. Porphyrins exhibit long-lived (>1 ns) π^* singlet excited states with only weak singlet/triplet mixing [116]. Their lowest and highest unoccupied molecular orbitals are located above the CB of TiO_2 and below the redox couple in the electrolyte solution, respectively. Thus, they meet the requirement for charge separation at the semiconductor/dye/electrolyte surface [127]. Porphyrins have a wide range of absorption that generally extends from the visible to near infrared region. They absorb strongly, with intense Soret bands (molar extinction coefficient = $10^5\,M^{-1}\,cm^{-1}$) in the blue visible spectrum and Q-bands (molar extinction coefficient = 10^4) in the green to red visible spectrum [113]. However, they have the disadvantage of an inherent tendency to aggregate, which reduces their efficiency as a sensitizer due to probable interaction between the excited and ground states.

To improve their efficiency, co-adsorbates such as poly(4-vinylpyridine) and chenodeoxycholic acid have been introduced [133,134]. Among various porphyrins used for the photosensitization of TiO_2, zinc derivatives are most common, including zinc 5-(4-carbomethoxyphenyl)-15-(4-carboxyphenyl)-10,20-bis-(pentafluorophenyl)-porphyrin (Fig. 13) and diphenylamine-substituted porphyrin dye. The latter has particularly been reported to hinder charge recombination [135]. To reduce charge recombination and enhance photocatalysis, the presence of electron donor groups can contribute to increasing the spatial separation between

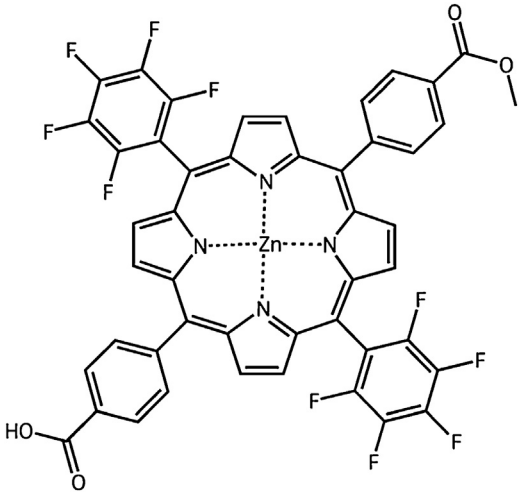

Fig. 13. Zinc 5-(4-carbomethoxyphenyl)-15-(4-carboxyphenyl)-10,20-bis-(pentafluorophenyl) porphyrin (ZnBPFP) [113].

the positive charge density created on the dye and the injected electrons in the photocatalyst [135].

Organic dyes

Organic dyes are the most widely studied sensitizers [117,136–139] because of their low cost relative to ruthenium-based sensitizers. Metal-free organic dyes are capable of highly efficient light harvesting over a wide spectral region of sunlight, with a molar extinction coefficient of 100,000 $M^{-1}\,cm^{-1}$ [140,141]. Organic dyes exhibit a variety of chemical structures, such as porphyrins, coumarines, catechol, polyenes, cyanines, hemicyanines, phthalocyanines, indolines, thiophenes, and polymeric dyes [40]. They have a characteristic D-π-A structure (Fig. 14) wherein the electron donating groups and electron accepting groups are connected through a π conjugate link. The link (thiophene units or phenylene vinylene units) can mediate the charge transport through the molecules. The acceptor group (cyanoacrylic acid) is

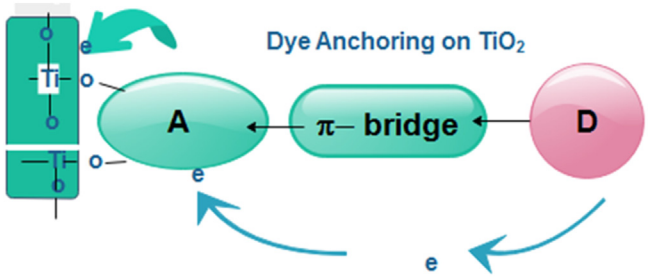

Fig. 14. Schematic of the D-π-A structure: an electron donating group and an electron accepting group are connected through a π conjugate link.

anchored to the metal oxide CB (the LUMO must be above CB of TiO_2) to facilitate electron injection.

Commonly used donor groups include indoline, N, *N*-dialkylaniline, and aminocoumarins. They have been incorporated into organic dyes for DSSCs and have shown efficiencies between 8 and 9.5% [142,143]. Although metal-free organic dyes have a higher molar extinction coefficient than porphyrins, they possess a similar tendency to aggregate. Strong intermolecular interactions cause π–π^* stacking of organic dye molecules. Co-adsorption of dye with additives [144,145] and structural modification of dye molecules [146] effectively prevent dye aggregation and improve efficiency.

Anchoring groups for photosensitizers and catalysts

Photosensitizes and catalysts have been coupled either directly to photoanodes or through the addition of anchoring groups. However, the latter can result in stronger bonding than the former [114]. Moreover, anchor groups coupled between a sensitizer and a photo anode can produce high surface coverage and strong electronic coupling between the occupied orbitals on the dye and the CB of the semiconductor, improving stability and performance [3,147]. Depending on the molecular dye, the anchoring can take place through various interactions, including covalent bonding, hydrogen bonding, electrostatic forces, hydrophobic interactions, van der Waals forces, and physical entrapment [40,114]. Different anchoring groups (catecholates, carboxylates, phosphonates, acetylacetonates, and hydroxamates, as shown in Fig. 15) have been used to bind photoactive and redox-active molecules to metal oxide surfaces [3].

The reaction variables (e.g., the pH, redox potential, and polarity of the solvent) can also affect the nature and number of anchoring groups coupled in the photo anode/sensitizer/catalyst system, which can affect the efficiency of the photosensitizer [99,135,148]. Consequently, an ideal anchoring group provides strong adsorption between various molecular species, and the photo anode can

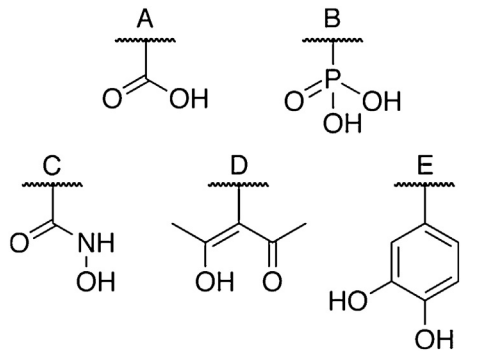

Fig. 15. Anchoring groups to bind molecular species to titanium dioxide: (A) carboxylic acid, (B) phosphonic acid, (C) hydroxamic acid, (D) 3-substituted-2,4-pentanedione (acetylacetonate), and (E) catechol [3].

facilitate fast electron transfer between the LUMO and the CB of the semiconductor while resisting aqueous and oxidation conditions.

The structures and optoelectronic performance of DSSC dyes with carboxylic and cyanoacrylic acid anchors have been reviewed extensively; for detailed information, see the work of Hagfeldt el al. [138]. Carboxylic anchoring is an effective coordinating compound for transition metal complexes in which MLCT dominates [149]. Because carboxylic anchoring compounds are bifunctional (that is, they have adsorption and electron withdrawal capabilities), photo-excited electrons from the CB of the semiconductor can be conducted more effectively than with a phosphonate anchoring group. Nonetheless, the latter offers stronger bonding to TiO_2 [3]. For example, when the surface desorption of ruthenium sensitizers was examined in aqueous solutions at pH 5.7, carboxylate and phosphonate anchors showed 90 and 30% desorption, respectively, under the same conditions [150,151]. Thus, phosphonates can act as more efficient anchoring groups than carboxylates. The low charge transfer rate of phosphonate groups has been attributed to the tetrahedral geometry of the phosphorus center and the loss of conjugation [152]. In addition to carboxylate and phosphonate anchoring groups, other groups (e.g., hydroxamic acid, acetylacetonate, and catechol) have also been explored [153–155]. A hydroxamic anchor group, for example, is highly stable and resists oxidative, neutral, and basic aqueous conditions; therefore, it offers favorable electron transfer [156].

Similarly, acetylacetonate derivatives have been cited for their outstanding coordination properties toward transition metals and their stability over a wide pH range; thus, they can be considered as alternative aqueous- and oxidative-stable anchor groups for photo anode/dye/catalyst systems [149]. Catechol has two charge transfer pathways, one through a transfer from the dye's excited state to the TiO_2 layer and the other from the dye's ground state to the CB of the TiO_2 [149]. However, in DSSC applications, the incident photon-to-current efficiency is relatively low (20%) because of strong parasitic recombination [157].

Electron transfer mediators

Clearly, current photovoltaic systems are more efficient than natural photosynthesis. Nonetheless, natural photosynthesis provides the inspiration for the design of efficient biomimetic systems. The overall efficiency of photosynthesis is less than 10% at low light levels and 1–3% in full sunlight [158,159]. In contrast, efficient crystalline silicon cells have an efficiency of about 24% [113]. However, it is important to mimic nature to understand the limitations of biological systems and to apply that knowledge to artificial systems to improve the efficiency associated with current commodity fuel sources (photovoltaics and DSSCs).

The reaction center for the water oxidation process in natural photosynthesis is the protein complex called photosystem II (PSII), which uses a form of chlorophyll known as P680. In photosynthesis, electron transfer is mediated through a redox-active tyrosine (tyrosine Z (TyrZ)-tyrosine D (TyrD))-histidine pair (TyrZ-D_1His190). Thus, direct electron transfer between the photo excited state of P680 (P680*) and the OEC does not exist in PSII [113]. The OEC is made up of an inorganic complex of one calcium and four manganese ions [160,161]. In a typical process, the photoexcitation of P680 to P680* produces an oxidizing equivalent. The highly oxidized and unstable P680* decays through electron transfer via an electron transport chain to the primary and secondary quinone cofactors Q_A and Q_B via a pheophytin primary electron acceptor at photosystem 1 (PS1) [13]. Electrons are then re-energized for their final purpose of either CO_2 fixation through the Calvin cycle or hydrogen production at the hydrogenase [162]. P680* is reduced by the tyrosine and loses its phenolic protons to a histidine group [13], and the tyrosine becomes a neutral tyrosine

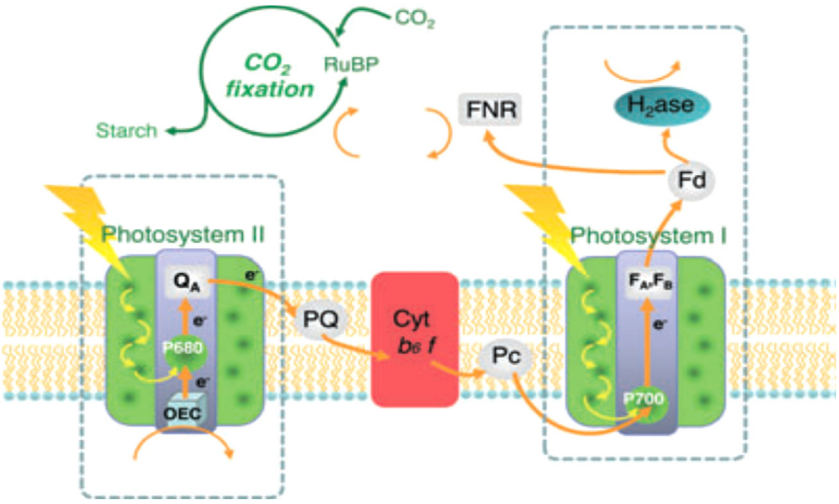

Fig. 16. Schematic of the photosynthetic chain in oxygenic photosynthesis, reproduced from [162].

radical in the process [13]. These tyrosyl radicals ($TyrZ^{*}$ and TyrD*) oxidize the OEC within microseconds [163], which offers the thermodynamic potential needed for the OEC to oxidize two water molecules from four photons and thereby induce charge separation events. Oxygen is produced in that process (Fig. 16), and the oxidized OEC relaxes back into its original oxidation state [13].

The use of mediators in artificial photosynthesis has received a lot of interest because biomimicry of the electron transfer mediator improves the PCET process [164–166]. For example, Johansson et al. prepared triads containing a $[Ru(bpy)_3]^{2+}$ core, a tyrosine ethyl ester, and a variety of electron acceptors [165]. They observed a charge separation yield of ~10%, with a fraction of the charge-separated states persisting for microseconds. Similarly, a molecular triad of a high-potential porphyrin, a tetracyanoporphyrin electron acceptor, and a benzimidazole-phenol secondary electron-donor was designed to mimic the tyrosine-histidine mediator architecture of PSII [13]. That system effectively induced charge separation that was thermodynamically able to oxidize water [13]. Thus, in principle, artificial photosynthesis can be designed to model PSII and thereby improve electron transfer in water splitting photocatalysis (details in Section "Water oxidation catalysts").

Water oxidation catalysts

An ideal WOC must be robust and stable near the thermodynamic potential for water, so it can facilitate the formation of dioxygen that remains active after approximately 10^9 cycles [3,113,167,168]. No catalyst has yet been reported to meet those criteria, although enormous research efforts have been made to design catalysts with improved performance. The importance of catalyst in water splitting cannot be overemphasized. The slow rate of water oxidation caused by a four-electron, four-proton process could be increased by the use of a catalyst that could facilitate the multiple-proton-coupled electron-transfer processes with low activation barriers [169,170].

Measuring the efficiency of a WOC is premised on three parameters: the turnover number (TON), turnover frequency (TOF), and over potential. The number of cycles that a catalyst goes through before becoming inactive is known as the TON [113]. The TON per unit time is called the TOF, and the additional energy (external bias) per unit charge needed to drive the process is described as the over potential [113]. A detailed discussion of WOCs is beyond the scope of this review, but interested readers can refer to several detailed reviews [113,167,171,172]. Generally, four WOCs have been integrated into dye-sensitized photo anodes: molecular catalysts, polyoxometalates, cubanes, and heterogeneous catalysts [113]. The most efficient molecular WOC is the naturally occurring complex of PSII. Inspired by nature, molecular catalysts have been produced from transition metals (Ru, Mn, and Ir) coordinated by organic ligands [173,174].

Molecular water oxidation catalysts

Molecular catalysts are interesting because of their ease of synthesis from abundant and cheap materials, high activity and tunability, and potential to be integrated into sophisticated molecular assemblies [174,175]. As homogeneous catalysts, they can be readily characterized structurally and are amenable to detailed kinetic/mechanistic studies [113]. However, molecular catalysts suffer from instability and complexity in their synthetic approaches because their organic ligands are thermodynamically unstable in the presence of O_2/air as they degrade into CO_2 and H_2O [167,172,173]. In addition to oxidation instability, molecular catalysts also suffer from both thermal and hydrolytic instability. A few notable examples of molecular WOCs are highlighted in Table 1. To date, the most widely studied transition metal in water oxidation molecular catalysts is ruthenium (Ru). Ru complex molecular catalysts have reasonable TOF (0.004–0.00675 s^1), TON (13–1690), and over potential (47–4280 mV vs NHE) and are considered ideal transitional metals (Table 3). Moreover, through the formation of stable metal–ligand bonds, Ru complexes can increase the stability of the reactive intermediates involved in water oxidation [176].

The first example of a molecular oxidation catalyst was the Ru^{III} dimer, $[(bipy)_2(H_2O)\,Ru^{III}\text{-}ORu^{III}\,(H_2O)\,(bipy)_2]^{4+}$, where bipy = 2, 2~-bipyridine (Table 3, Fig. 16). This complex generates oxygen at rates of 0.004 molecules O_2 s^{-1}, for an average of 13 turnovers when $Ce^{(IV)}$ is the sacrificial oxidant [177]. The TOF, TON, and over potential of the Ru complex (Table 3) are 0.004–0.00675 s^1, 13–1690, and 280 mV vs NHE, respectively. Compared to ruthenium, iridium$^{(III)}$-centered molecular catalysts appear more promising, with improved values for TOF (0.04 s^1) and TON (2490) and a low over potential (185 mV vs NHE) (Table 3, Fig. 17). They consist of a single Ir^{III} center supported by two phenyl pyridines and two water ligands, $[Ir\ (R_1R_2\text{phenylpyridine})_2(H_2O)_2]^{+}$, with Ce^{4+} as the sacrificial oxidant [178].

Table 3
Comparison of selected molecular water oxidation catalysts [113].

Order	Catalyst	Oxidant	TOF (s^{-1})	TON	Over potential (mV vs. NHE)	Refs.
A: Molecular water oxidation catalysts						
1	*cis,cis*-$[Ru(bpy)_2(H_2O)]^2(\mu\text{-}O)^{4+}$	$Ce^{(IV)}$	0.004	13	474	[177]
2	*in, in*-$[(Ru(tpy)(H_2O)]^2(\mu\text{-bpp})^{3+}$	$Ce^{(IV)}$	0.86	512		[249]
3	*trans, trans*-$[Ru_2(L_1)(4\text{-}CH_3O\text{-}py)_4Cl]^{3+}$	$Ce^{(IV)}$	3.8×10^{-5}	689		[250]
4	$[Ru_2(L_2)(4\text{-}CH_3\text{-}py)_6]^{1+}$	$Ce^{(IV)}$	0.24	1690	424	[251]
5	$[Ru_2(L_3)(4\text{-}CH_3\text{-}py)_4Cl]^{1+}$	$Ce^{(IV)}$	1.2	10 400	330	[252]
6	$[Ru(tpy\text{-}PO_3H_2)(H_2O)_2]_2O^{4+}$	1.25–1.5V vs. Ag/AgCl		1.8	414	[253]
7	$[Ru_2(OH)(3,6\text{-t Bu}_2qui)_2(btpyan)]^{2+}$	1.7V vs. Ag/AgCl	0.232	33 500	405	[254]
8	*trans*-$[Ru(L_4)(4\text{-}CH_3\text{-}py)_2(H_2O)]^{2+}$	$Ce^{(IV)}$	0.0028	260		[255]
9	$[Ru(tpy)(bpm)(OH_2)]^{2+}$	$Ce^{(IV)}$	0.019	7.5	377	[256]
10	$[Ru(Mebimpy)(bpy)(OH_2)]^{2+}$	$Ce^{(IV)}$	0.0067	7.5	280	[257]
11	$[Ir(ppy)_2(OH_2)_2]^+$	$Ce^{(IV)}$	0.004	2490	185	[178]
B: Polyoxometalates						
12	$[Ru_4(\mu\text{-}O)_4(\mu\text{-}OH)_2(H_2O)_4(\gamma SiW_{10}O_{36})_2]^{10-}$	$Ce^{(IV)}$	0.131	500	246	[188]
13	$[Ru_4(\mu\text{-}O)_4(\mu\text{-}OH)_2(H_2O)_4(\gamma\text{-}SiW_{10}O_{36})_2]^{10-}$	$[Ru(bpy)_3]^{2+}/S_2O_8{}^{2-}$	0.08	350		[258]
14	$[Ru_4(\mu\text{-}O)_5(\mu\text{-}OH)(H_2O)_4(\gamma\text{-}PW_{10}O_{36})_2]^{9-}$	$[Ru(bpy)_3]^{2+}/S_2O_8{}^{2-}$	0.13	120	248	[259]
15	$[Co_4(H_2O)_2(PW_9O_{34})_2]^{10-}$	$[Ru(bpy)_3]^{2+}/S_2O_8{}^{2-}$	0.0013	224	441	[173]
16	$[Co_4(\mu\text{-}OH)(H_2O)_3(SiW_{19}O_{70})^2]^{11-}$	$[Ru(bpy)_3]^{2+}/S_2O_8{}^{2-}$	0.1	80		[183]
17	$[(IrCl_4)KP_2W_{20}O_{72})]^{14-}$	$[Ru(bpy)_3]^{3+}$	0.0292	5.25	215	[260]
18	$[Ru(H_2O)SiW_{11}O_{39}]^{5-}$	$Ce^{(IV)}$	0.003	20	188	[261]
19	$[Co_2Mo_{10}O_{38}H_4]^{6-}$	$[Ru(bpy)_3]^{2+}/S_2O_8{}^{2-}$	0.171	154	350	[262]
20	$[CoMo_6O_{24}H_6]^3$-	$[Ru(bpy)_3]^{2+}/S_2O_8{}^{2-}$	0.119	107	420	[262]
C: Cubane catalysts						
21	$[Mn_4O_4L_6]^+$	1V vs. Ag/AgCl	0.075–0.005	>1000	380	[263]
22	$Co^{III}{}_4O_4(OAc)_4(py)_4$	$[Ru(bpy)_3]^{2+}/S_2O8]^{2-}$	0.02	40	332	[192]
D: Heterogeneous catalysts						
23	RuO_2	$[Ru(bpy)_3]^{2+}/[Co(NH_3)_5Cl]^{2+}$	0.052	68	310	[264]
24	RuO_2 (5 nm)	$[Ru(bpy)_3]^{2+}/S_2O_8{}^{2-}$	0.0045	19.2	310	[202]
25	RuO_2 (10 nm)	$[Ru(bpy)_3]^{2+}/S_2O_8{}^{2-}$	0.089	2.7	310	[202]
26	Rutile RuO_2 (6 ± 2 nm)	1.48V vs. RHE	≥0.000069		280	[201]
27	$IrOx.nH_2O$	$[Ru(bpy)_3]^{2+}/S_2O_8{}^{2-}$	0.0004	3	310	[199]
28	Citrate-$IrOx.nH_2O$ (20 nm)	$[Ru(bpy)_3]^{2+}/S_2O_8{}^{2-}$	0.05	80	330	[265]
29	Succinate-$IrOx.nH_2O$	$[Ru(bpy)_3](PF_6)_2/S_2O_8{}^{2-}$	0.049	28	330	[266]
30	$IrOx.nH_2O$	1.4V vs. Ag/AgCl	4.71		220	[267]
31	Co_3O_4	$[Ru(bpy)_3]^{2+}/S_2O_8{}^{2-}$	0.035		325	[268]

Bpy: bipyridine; tpy: terpyridine; bpp: bis (2-pyridyl)-3, 5-pyrazolate; L1: 6-bis [6′-(1′, 8′-napthyrid-2′-yl) pyrid-2′-yl] - pyridazine; 4-CH3O-py: 4-methoxypyridine; L2: 3, 6-bis-(6′-carboxypyrid-2′-yl)-pyridazine; 4-CH3-py: 4-methylpyridine; L3: 1, 4-bis (6′-COOH-pyrid-2′-yl) phthalazine; tpy-PO3H2: 4′-phosphonato-2,2′:6′,2′-terpyridine; 3,6-t Bu2qui: 3,6-di-tert-butyl-1,2-semiquinone; btpyan: 1,8-bis(2,2′:6′,2′-terpyridyl) anthracene; L4: 4-tert-butyl-2, 6-di ([1′, 8′]-naphthyrid-2′-yl) pyridine; bpm: 2, 2′-bipyrimidine; Mebimpy: 2, 6-bis (1-methylbenimidazol); 11L: di-(p-methyoxyphenyl)-phosphine; OAc: acetate; py: pyridine.

Polyoxometalate water oxidation catalysts

Molecular WOCs suffer from limitations such as oxidative, thermal, and hydrolytic instability. Therefore, many research groups have investigated polyoxometalate (POM)-based WOCs [167,172,179–183]. POMs are early transition metal oxygen anion clusters that form spontaneously in water when the contents of soluble transition metals, molecular monomeric transition metal precursors ($WO_4{}^{2-}$), and insoluble metal hydroxides or hydrated oxides (WO_3 hydrate and V_2O_5) are adjusted to the appropriate pH [184–186]. POMs are entirely inorganic WOC catalysts devoid of carbon-containing bonds. Therefore, they are stable against heat, aqueous medium, and corrosive environments. The most abundant and efficient POMs are polytungstates, $W^{(VI)}$> polymolybdates, $Mo^{(VI)}$> polyvanadates, $V^{(V)}$> polyniobates, $Nb^{(V)}$> polytantalates, $Ta^{(V)}$ [172]. Those metal frameworks form either acid- or base-stable polyanions. Specifically, polytungstates, $W^{(VI)}$; polymolybdates, $Mo^{(VI)}$; and polyvanadates, $V^{(V)}$ form acid-stabilized polyanions, whereas polyniobates, $Nb^{(V)}$ and polytantalates, $Ta^{(V)}$ are basic-stabilized polyanions [167,172]. The POMs readily facilitate

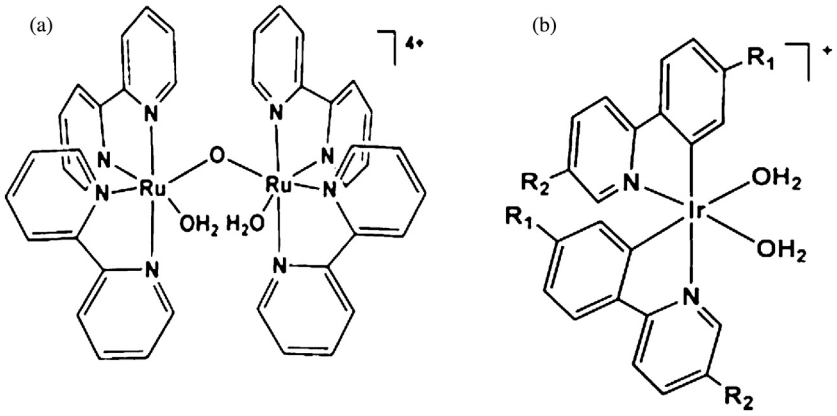

Fig. 17. Examples of ruthenium and iridium molecular catalysts: (a) $[(bipy)_2\ (H_2O)\ Ru^{III}O\ Ru^{III}\ (H_2O)(bipy)_2]^{4+}$ and (b) $[Ir(R_1R_2phenylpyridine)_2(H_2O)_2]^+$ [176].

the water splitting redox reaction by reducing protons to produce hydrogen gas and oxidizing water to produce oxygen. Thus, POMs can meet most of the conditions required for an ideal WOC.

Table 3 shows a comparison of POMs that have been studied recently for water oxidation. The polyoxometalate structure, consisting of a tetra ruthenium core stabilized by a metal framework complex ($[Ru_4(\mu\text{–}O)_4(\mu\text{–}OH)_2(H_2O)_4(\gamma\text{–}SiW_{10}O_{36})_2]^{10-}$ (Ru_4SiPOM)), has been studied for water splitting [187,188]. Different groups of chemical oxidants were studied, particularly cerium (IV) oxide, tris(bipyridine) ruthenium (II) chloride, and peroxodisulphate (VI) ions ($Ce^{(IV)}$, $[Ru(bpy)_3]^{2+}$, and $S_2O_8^{2-}$). The catalytic activity of $Ce^{(IV)}$ had a TON of 500 without apparent loss of catalytic activity and an O_2 yield of 90% [113]. However, when $[Ru(bpy)_3]^{2+}$ and S_2O_8 were used, TONs up to 350 and a TOF of 0.08 were observed (Table 1). A related work investigated the catalytic activity of the phosphorous-containing analogue $[Ru_4(\mu\text{–}O)_5(\mu\text{–}OH)(H_2O)]^{4-}$ $(\gamma\text{–}PW_{10}O_{36})_2]^{9-}$ (Ru_4P-POM) [113]. Although Ru_4PPOM could oxidize water, its rate of photo-driven water oxidation was approximately 70% (Table 1) [113]. Therefore, cerium (IV) oxide appears to be a more effective oxidant than tris(bipyridine) ruthenium (II) chloride or peroxodisulphate (VI) ions.

Cubane water oxidation catalysts

Most homogenous and heterogeneous WOCs use noble metals (ruthenium, iridium, or rhodium) as their metal framework. Cubane catalysts instead use cheap and earth-abundant elements. Cubane is a homogeneous catalyst based on the cuboidal structure of the active manganese calcium oxide cluster ($CaMn_4$) core found in PSII [113,189–192]. Cubane has the general core structure of $[M_4O_4]^{6+ \text{ or } 4+}$ with six to eight bidentate ligands for coordination [113]. Table 3 compares cubane ($[Co^{III}{}_4O_4(Ac)_4(pyr)_4]$) with a Nafion-polymer-immobilized Mn_4O_4 cubane. The Nafion-polymer-supported Mn_4O_4 ($(p\text{-}OMe\text{–}C_6H_4)PO_2)_6$ cubane showed a sustained water oxidation photocurrent over a period of 10 h under UV illumination. A TON greater than 1000 turnovers was reported, whereas the TON for the ($[Co^{III}{}_4O_4(Ac)_4(pyr)_4]$) cubane was only 40.

Heterogeneous water oxidation catalysts

Heterogeneous WOCs are either colloidal suspensions of nanoparticles or electrochemically deposited films. They are mainly made of noble metal oxides (RuO_2, $NiCo_2O_4$, iridium oxides, and IrO_2). Compared to homogeneous WOCs, heterogeneous nanoparticle-based catalysts are chemically stable and easy to prepare [113]. Research has demonstrated that these catalysts have low oxidation over potential and excellent faradaic efficiency and effectiveness as WOCs [193–197]. Mononuclear iridium complexes able to oxidize water into dioxygen were first reported in 2008 [178]. The catalytic cycle was driven using $Ce^{(IV)}$ as a chemical oxidant, and the work explored the role of ligand modification in the activities and lifetimes of catalysts (Fig. 18) [174]. It is interesting to note that the TOFs varied from less than 4 to 16 h^{-1}, with a high TON of 2760. Since then, crystalline IrO_2 and amorphous colloidal $IrOx.nH_2O$ (Table 1), which have a low over potential (200–300 mV), have been investigated as highly active WOCs over a wide pH range [198–200].

The potential of colloidal RuO_2 as a WOC, driven by a chemical oxidant such as $Ce_{(IV)}$ or $[Ru(bpy)_3]^{3+}$ or photochemically with $[Ru(bpy)_3]^{2+}/S_2O_8^{2-}$ or $[Co(NH_3)_5Cl]^{2+}$, has also been studied (Table 3) [201–203]. Although RuO_2 exhibited enhanced performance (e.g., in terms of over potential (310 mV vs. NHE), TOF (0.05 s^{1}), and chemical stability under catalyst cathodic conditions), it corroded under oxidizing conditions [113,204]. Consequently, it is non-ideal as a WOC.

Complete system assembly

So far, we have discussed the unit components of the artificial photosynthetic water splitting process. The challenge is to construct a device for solar fuel production that optimizes the processes of light harvesting, electron injection, and charge transport while ensuring that improvements in one process do not significantly interfere with the performance of the other two [3,205]. In this regard, Gust et al. designed a photo-electrochemical cell for water splitting to meet the basic requirements [23]. This cell (Fig. 19) uses TiO_2 (photo anode) coupled with a phosphonate anchoring group and a ruthenium-based chromophore that can absorb visible light. When the ruthenium complex is irradiated, electrons from the LUMO hop into the CB of the TiO_2 to activate charge separation. The injected electrons are conducted through the wire to the cathode, where protons are reduced to hydrogen. The other side of the ruthenium polypyridyl dye is anchored to a heterogeneous WOC ($IrO_2 nH_2O$) via a malonate moiety. The oxidized ruthenium dye is reduced by iridium oxide nanoparticles, regenerating the sensitizer and accumulating the oxidation

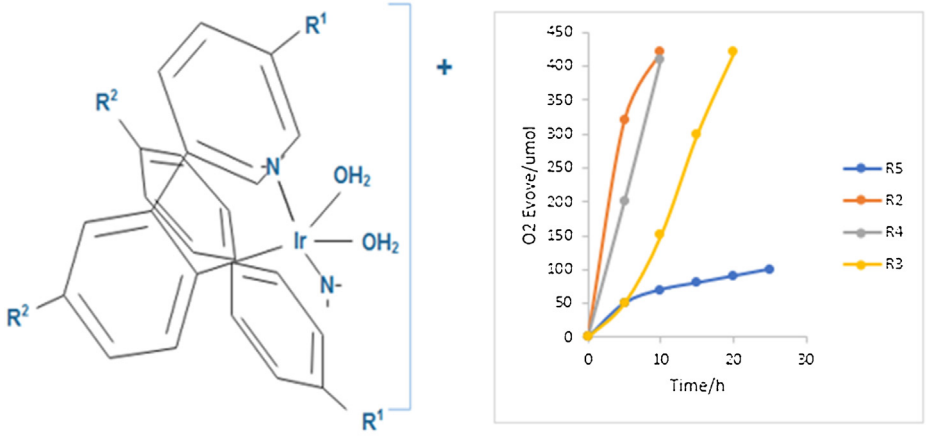

1 R^1, R^2: -H, 2 R^1: CH_3, R^2: -H, 3 R^1: -CH3, R^2: -Ph, 4 R^1: -CH3, R^2: -F, 5 R^1: -CH3, R^2: -Cl

Fig. 18. Ligand substitution in the $[Ir(ppy)_2(OH_2)_2]$ MOF framework (left). Mononuclear iridium complexes produce a distinct structure-activity relationship with the rate of oxygen production (right) [174].

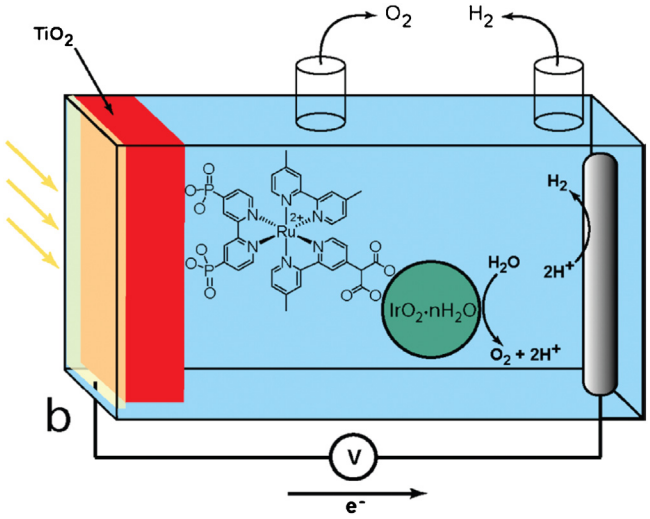

Fig. 19. Schematic of an artificial photosynthetic water splitting cell to generate hydrogen [23].

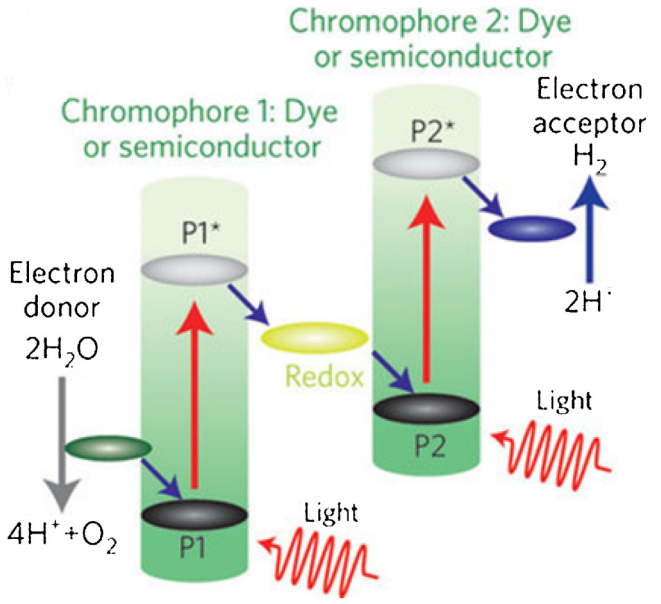

Fig. 20. Two-step (Z-scheme) reactions, P1: the first chromophore in a two-step reaction system; P1*: excited state of P1; P2: second chromophore in a two-step reaction system; P2*: excited state of P2 [31].

potential on the nanoparticle for water oxidation to O_2 [205]. Thus, the complete system mimics the ruthenium functions of the natural photosynthetic antenna (light absorption) and reaction center (photo-induced electron transfer) for electron–hole separation [23].

For photo-induced water splitting to be effective, the basic functions of the catalyst (e.g., reaction center function, proton reduction catalyst, and water oxidation capacity) need to be optimized because the quantum yield of water splitting is low (0.9%). In addition, the solar spectrum of interest for water splitting involves photons with a wavelength range of 1000 nm because the energy barrier for the thermodynamic conversion of water to oxygen and hydrogen is 1.23 eV [31]. However, the chlorophyll and other chromophores (ruthenium complexes and porphyrins) used as light harvesters in both natural and artificial photosynthesis absorb in the range of 500–680 nm. Thus, only about 45% of the spectrum is useful, and the rest remains elusive [23]. Again, kinetics impose restrictive limits on the process because the forward reaction (injection of electrons into the semiconductor) competes with the backward reaction (electron hole recombination) (see Section "Band gap engineering") [40]. For the forward reaction to compete favorably with the backward reaction, the process requires a significant thermodynamic driving force. Additionally, catalysts for both water oxidation and proton reduction require over potential (activation energy 1.23 eV vs. NHE or $\Delta G = 475$ kJ/mol) or an external bias to function [23].

An ideal strategy for designing an efficient water splitting system is to have an antenna that absorbs photons at wavelengths >1000 nm. Again, such a system must be similar to the tandem systems in the reaction centers of photosystems I and II (PS700 and PS680, respectively) in natural photosynthesis [23]. Such a tandem arrangement (also known as the Z scheme, Fig. 20) has been implemented in systems based on inorganic semiconductors for water splitting and DSSCs [23,31,206]. Unfortunately, the absorption spectra of photosystems I and II do not complement each other. The potentials generated by the two photosystems do not add linearly, and only photons with wavelengths ≤ 680 nm actually contribute to the light absorption process [23]. In an artificial photosynthetic device, it would be better to engineer the two photosystems such that one reaction center absorbs from 400 to 700 nm to generate the redox potential necessary to oxidize water, and the second photosystem absorbs from 700–1000 nm to generate the potential needed to drive the catalytic reduction of hydrogen ions into hydrogen gas [23]. Again, to ensure effective electron transfer from the OEC to the oxidized primary electron-donor chlorophyll (P680*), the electron transfer must be mediated by a redox-active tyrosine-histidine pair between the dye and WOC. PCET is effective for coupling the oxidizing and reducing equivalents formed by the reaction centers of the catalysts for water oxidation or hydrogen gas production [207,208].

Finally, both WOCs and WRCs must fulfil the requirements for a good catalyst (see Section "Water oxidation catalysts"). WRCs that have been investigated so far include iridium, rhodium, ruthenium, and platinum [54,171,209]. Although these catalysts are effective and function with relatively low over potential, they are expensive when deployed in bulk artificial photosynthetic systems for hydrogen production [23,171]. Earth abundant metals (Co, Fe, Ni, etc.) can be used as substitute photocathodes instead of expensive platinum in water splitting proton reduction [210]. Living organisms produce hydrogen using some of the catalysts contained in the enzyme hydrogenase. In fact, hydrogenases have been used directly as catalysts in artificial photosynthesis to produce hydrogen gas [211,212]. However, because hydrogenases are large, complex enzymes, they are sensitive to deactivation by oxygen. Thus, they are not ideal catalysts for artificial photosynthetic hydrogen production [23]. In contrast, cobalt hangman porphyrins have recently been identified as effective catalysts for the hydrogen evolution reaction (HER) [213]. The hangman porphyrins facilitate HER by directly mediating PCET reactions to generate H_2 gas.

Current shortcomings and outlook

After a thorough review of the recently published literature in the field of solar photocatalysis, we recognized that, despite significant advances, current materials remain far from an ideal or practical solution. The three main shortcomings of existing materials are low quantum efficiency, a high rate of charge carrier recombination, and long-term chemical/physical instability.

Low quantum efficiency in this context applies to most traditional materials with large band gaps (>3.0 eV). Although that enables them to generate highly energetic charge carriers, they can use only UV radiation; which is a meager 5% of the available terrestrial energy. On the other hand, visible light accounts for approximately 40% of the incoming solar energy

that could be tapped. Most materials with an appropriate band gap are derived from transition metal compounds, which have stability issues. A possible solution to that problem lies in the effective use of a synergistic effect between high and low band gap semiconductors. If materials with dissimilar energy levels are joined through a heterojunction, one material acts as a sensitizer (low band gap) for the other (high band gap). Thus, charge carriers can be generated using visible light. Furthermore, a suitable structural arrangement (core-shell or Janus) imparts a higher stability to the composite as a whole. In that way, both problems could be addressed within a single material. Another promising way to address those problems could be through plasmonic photocatalysis. However, until the problems of high fabrication and material costs are solved, practical applications in that field will be limited.

Similarly, possessing a higher quantum efficiency would contribute little if the generated charge carriers are lost to bulk or surface recombination, depending on the morphology of the material. Bulk recombination can be largely suppressed by reducing the particle size of the catalyst, which also imparts the additional benefit of increasing its effective surface area. However, because small particles are prone to a high rate of back reactions (against the forward reaction), they are difficult to recover and pose a nanoparticle hazard. A suitable mechanism allowing easy recovery of the particles post reaction, such as a suitable membrane for the immobilization of the catalyst (embedded structure), could greatly alleviate that problem. Another interesting method would be the incorporation of magnetic materials that impart the dual benefit of acting as a suitable co-catalyst and providing easy magnetic separation. Surprisingly, only a few studies have reported such approaches. However, they can serve as a proof of concept to indicate the immense potential for improvement.

The third and most significant problem lies in catalyst stability against photo-corrosion, galvanic corrosion, and poisoning. The problem can be further aggravated by the reusability of the catalyst over many cycles. Although a number of papers are published every year in the field of photocatalysis, only a few ever report the long-term stability of the catalyst. This deficiency could partially result from the lack of testing standards in this field, which is also responsible for the lack of comparative data in the literature. It would be highly beneficial for the scientific community to attain a consensus regarding the testing and reporting parameters for catalysts, with stability studies being a major part. That would make it easy to root out superficial and impractical approaches in favor of promising novel candidates. The nature of the existing limitations makes it highly improbable that a single-component material will satisfy all of the required criteria. Therefore, multicomponent heterogeneous systems probably hold the key to the development of a practical and scalable catalytic material.

Conclusions

Optimizing a complete water splitting system to maximize efficiency for commercial purposes remains a scientific challenge. However, with much effort and many advances in the field, the challenges of the light-harvesting process and charge separation in PSI and II, PCET, and the redox reactions at both the OEC and WRC will hopefully be resolved sooner than later.

In this work, we offered a comprehensive review of recent advances in photo anode semiconductors, light harvesting sensitizers, WOCs, PCET via electron transport mediators, and a complete system assembly able to complete the four-electron water-oxidation reaction for efficient photocatalytic water splitting. Overall, the conversion efficiency of light energy in storable form (chemical bonds) and photo-induced water purification cannot be over emphasized. The challenge for future work lies in the ability to design compact system assemblies, particularly systems that coordinate a photosensitizer and catalyst to transfer four oxidizing equivalents and generate the dioxygen and hydrogen gas required for commercial applications.

Acknowledgements

Henry Agbe acknowledges support from the Commonwealth Scholarship Commission in the UK (CSC); support from the materials chemistry group of the Materials Science and Metallurgy Department-University of Cambridge is also deeply appreciated. The authors also thank the African Materials Science and Engineering Network for its financial support. DDA acknowledges support by the University of Ghana BANGA-Africa programme. KHK acknowledges support from a grant from the National Research Foundation of Korea (NRF) funded by the Ministry of Science, ICT, & Future Planning (Grant No: 2016R1E1A1A01940995).

References

[1] G.F. Moore, G.W. Brudvig, Annu. Rev. Condens. Matter Phys. 2 (2011) 303.
[2] F. Birol, Aust. Econ. Rev. 39 (2006) 190.
[3] K.J. Young, L.A. Martini, R.L. Milot, R.C. Snoeberger, V.S. Batista, C.A. Schmuttenmaer, R.H. Crabtree, G.W. Brudvig, Coord. Chem. Rev. 256 (2012) 2503.
[4] T. Faunce, S. Styring, M.R. Wasielewski, G.W. Brudvig, A.W. Rutherford, J. Messinger, A.F. Lee, C.L. Hill, M. Fontecave, D.R. MacFarlane, Energy Environ. Sci. 6 (2013) 1074.
[5] M.M. Haque, D. Bahnemann, M. Muneer, Photocatalytic Degradation of Organic Pollutants: Mechanisms and Kinetics, INTECH Open Access Publisher, 2012.
[6] N. Wu, Nanoscale 10 (2018) 2679.
[7] F. He, DEStech Transactions on Environment Energy and Earth Science, (2017) .
[8] N. Raza, K.-H. Kim, H. Agbe, S.K. Kailasa, J.E. Szulejko, R.J. Brown, Asian J. Atmos. Environ. 11 (2017) 217.
[9] V. Shrivastava, Arch. Appl. Sci. Res. 4 (2012) 1244.
[10] R. Abe, K. Hara, K. Sayama, K. Domen, H. Arakawa, J. Photochem. Photobiol. A: Chem. 137 (2000) 63.
[11] R.B. Wang, S. Kørbel, S. Saha, S. Botti, N.V. Skorodumova, J. Phys. Chem. C 121 (2017) 9528.
[12] A. Fujishima, K. Honda, Nature 238 (1972) 37.
[13] J.D. Megiatto, A. Antoniuk-Pablant, B.D. Sherman, G. Kodis, M. Gervaldo, T.A. Moore, A.L. Moore, D. Gust, Proc. Natl. Acad. Sci. 109 (2012) 15578.
[14] A. Kudo, Y. Miseki, Chem. Soc. Rev. 38 (2009) 253.
[15] R. Nakamura, T. Tanaka, Y. Nakato, J. Phys. Chem. B 109 (2005) 8920.
[16] G. Liu, L.C. Yin, P. Niu, W. Jiao, H.M. Cheng, Angew. Chem. Int. Ed. 52 (2013) 6242.
[17] G. Liu, P. Niu, L. Yin, H.-M. Cheng, J. Am. Chem. Soc. 134 (2012) 9070.
[18] F. Wang, W.K.H. Ng, C.Y. Jimmy, H. Zhu, C. Li, L. Zhang, Z. Liu, Q. Li, Appl. Catal. B Environ. 111 (2012) 409.
[19] P. Zeng, X. Ji, Z. Su, S. Zhang, RSC Adv. 8 (2018) 20557.
[20] C. Huang, C. Chen, M. Zhang, L. Lin, X. Ye, S. Lin, M. Antonietti, X. Wang, Nat. Commun. 6 (2015) 7698.
[21] H. Wang, S. Jiang, W. Shao, X. Zhang, S. Chen, X. Sun, Q. Zhang, Y. Luo, Y. Xie, J. Am. Chem. Soc. 140 (2018) 3474.
[22] H. Ou, L. Lin, Y. Zheng, P. Yang, Y. Fang, X. Wang, Adv. Mater. 29 (2017) 1700008.
[23] D. Gust, T.A. Moore, A.L. Moore, Faraday Discuss. 155 (2012) 9.
[24] J. Sessler, A. Gebauer, E. Vogel, K. Kadish, K. Smith, R. Guilard, Kadish, K.M., (2000) 257–278.
[25] T.J. Meyer, Acc. Chem. Res. 22 (1989) 163.
[26] N.P. Redmore, I.V. Rubtsov, M.J. Therien, J. Am. Chem. Soc. 125 (2003) 8769.
[27] D. Gust, T.A. Moore, A.L. Moore, Acc. Chem. Res. 34 (2001) 40.
[28] Y.J. Jang, M.D. Bhatt, J. Lee, S.H. Choi, B.J. Lee, J.S. Lee, Advanced Energy Materials (2018)1702636.
[29] E. Edri, S. Aloni, H. Frei, ACS Nano 12 (2018) 533.
[30] M. Antonietti, A. Savateev, The Chemical Record, (2018) .
[31] Y. Tachibana, L. Vayssieres, J.R. Durrant, Nat. Photonics 6 (2012) 511.
[32] J. Kumar, A. Bansal, Photocatalysis by nanoparticles of titanium dioxide for drinking water purification: a conceptual and state-of-art review, Trans Tech Publ, 2013 p.130.
[33] Y. Sun, W.D. Chemelewski, S.P. Berglund, C. Li, H. He, G. Shi, C.B. Mullins, ACS Appl. Mater. Interfaces 6 (2014) 5494.
[34] S. Hoang, S.P. Berglund, R.R. Fullon, R.L. Minter, C.B. Mullins, J. Mater. Chem. A 1 (2013) 4307.
[35] J. Yu, X. Yu, B. Huang, X. Zhang, Y. Dai, Cryst. Growth Des. 9 (2009) 1474.

[36] T. Jafari, E. Moharreri, A.S. Amin, R. Miao, W. Song, S.L. Suib, Molecules 21 (2016) 900.
[37] A. Kryczyk, P. Żmudzki, U. Hubicka, Biomed. Chromatogr. (2017).
[38] K. Pstrowska, B.M. Szyja, H. Czapor-I, rzabek, A. Kiersnowski, J. Walendziewski, Photochem. Photobiol. 93 (2017) 558.
[39] D.D. Dionysiou, G.L. Puma, J. Ye, J. Schneider, D. Bahnemann, Photocatalysis: applications, Royal Society of Chemistry, 2016.
[40] J.M. Coronado, F. Fresno, M.D. Hernández-Alonso, R. Portela, Design of advanced photocatalytic materials for energy and environmental applications, Springer, 2013.
[41] A. Ishikawa, T. Takata, J.N. Kondo, M. Hara, K. Domen, J. Phys. Chem. B 108 (2004) 11049.
[42] R. Abe, T. Takata, H. Sugihara, K. Domen, Chem. Lett. 34 (2005) 1162.
[43] R. Asahi, T. Morikawa, T. Ohwaki, K. Aoki, Y. Taga, Science 293 (2001) 269.
[44] S.U. Khan, M. Al-Shahry, W.B. Ingler, Science 297 (2002) 2243.
[45] T. Umebayashi, T. Yamaki, H. Itoh, K. Asai, Appl. Phys. Lett. 81 (2002) 454.
[46] M. Jakob, H. Levanon, P.V. Kamat, Nano Lett. 3 (2003) 353.
[47] S. Sakthivel, M. Shankar, M. Palanichamy, B. Arabindoo, D. Bahnemann, V. Murugesan, Water Res. 38 (2004) 3001.
[48] M.R. St. John, A.J. Furgala, A.F. Sammells, J. Phys. Chem. 87 (1983) 801.
[49] V. Subramanian, E. Wolf, P.V. Kamat, J. Phys. Chem. B 105 (2001) 11439.
[50] I.-H. Tseng, J.C. Wu, H.-Y. Chou, J. Catal. 221 (2004) 432.
[51] K. Gurunathan, P. Maruthamuthu, M. Sastri, Int. J. Hydrogen Energy 22 (1997) 57.
[52] K. Dhanalakshmi, S. Latha, S. Anandan, P. Maruthamuthu, Int. J. Hydrogen Energy 26 (2001) 669.
[53] A.K. Jana, J. Photochem. Photobiol. A: Chem. 132 (2000) 1.
[54] A.S. Polo, M.K. Itokazu, N.Y.M. Iha, Coord. Chem. Rev. 248 (2004) 1343.
[55] X. Li, X. Chen, H. Niu, X. Han, T. Zhang, J. Liu, H. Lin, F. Qu, J. Colloid Interf. Sci. 452 (2015) 89.
[56] N. Serpone, J. Phys. Chem. B 110 (2006) 24287.
[57] S. Sridhar, T. Arunnellaiappan, N. Rameshbabu, S. Mika, A. Viswanathan, Surf. Eng. 33 (2017) 779.
[58] L. Matějová, K. Kočí, I. Troppová, M. Šihor, M. Edelmannová, J. Lang, L. Čapek, Z. Matěj, P. Kuśtrowski, L. Obalová, J. Nanosci. Nanotechnol. 18 (2018) 688.
[59] N.T. Nolan, D.W. Synnott, M.K. Seery, S.J. Hinder, A. Van Wassenhoven, S.C. Pillai, J. Hazard. Mater. 211 (2012) 88.
[60] M. Pelaez, B. Baruwati, R.S. Varma, R. Luque, D.D. Dionysiou, Chem. Comm. 49 (2013) 10118.
[61] G. Liu, H.G. Yang, X. Wang, L. Cheng, J. Pan, G.Q. Lu, H.-M. Cheng, J. Am. Chem. Soc. 131 (2009) 12868.
[62] S. In, A. Orlov, R. Berg, F. García, S. Pedrosa-Jimenez, M.S. Tikhov, D.S. Wright, R.M. Lambert, J. Am. Chem. Soc. 129 (2007) 13790.
[63] J. Wang, D.N. Tafen, J.P. Lewis, Z. Hong, A. Manivannan, M. Zhi, M. Li, N. Wu, J. Am. Chem. Soc. 131 (2009) 12290.
[64] V. Etacheri, C. Di Valentin, J. Schneider, D. Bahnemann, S.C. Pillai, J. Photochem. Photobiol. C: Photochem. Rev. 25 (2015) 1.
[65] C. Di Valentin, G. Pacchioni, A. Selloni, S. Livraghi, E. Giamello, J. Phys. Chem. B 109 (2005) 11414.
[66] A. Sclafani, J. Herrmann, J. Phys. Chem. 100 (1996) 13655.
[67] Y. Do, W. Lee, K. Dwight, A. Wold, J. Solid State Chem. 108 (1994) 198.
[68] M. Ni, M.K. Leung, D.Y. Leung, K. Sumathy, Renewable Sustainable Energy Rev. 11 (2007) 401.
[69] M. Anpo, M. Takeuchi, J. Catal. 216 (2003) 505.
[70] Z. Lian, W. Wang, G. Li, F. Tian, K.S. Schanze, H. Li, ACS Appl. Mater. Interfaces 9 (2017) 16959.
[71] A. Zielińska-Jurek, M. Klein, J. Hupka, Sep. Purif. Technol. 189 (2017) 246.
[72] M.M. Abdoul-Latif, J. Xu, J.X. Yao, S.Y. Dai, Au Nanoparticles Doped TiO2 Mesoporous Perovskite Solar Cells, Trans Tech Publ, 2017 p.18.
[73] K. Sayama, K. Yase, H. Arakawa, K. Asakura, A. Tanaka, K. Domen, T. Onishi, J. Photochem. Photobiol. A: Chem. 114 (1998) 125.
[74] N.-L. Wu, M.-S. Lee, Int. J. Hydrogen Energy 29 (2004) 1601.
[75] V. Subramanian, E.E. Wolf, P.V. Kamat, J. Phys. Chem. B 107 (2003) 7479.
[76] G.R. Bamwenda, S. Tsubota, T. Nakamura, M. Haruta, J. Photochem. Photobiol. A: Chem. 89 (1995) 177.
[77] M.K. Seery, R. George, P. Floris, S.C. Pillai, J. Photochem. Photobiol. A: Chem. 189 (2007) 258.
[78] R.S. Hyam, J. Jeon, S. Chae, Y.T. Park, S.J. Kim, B. Lee, C. Lee, D. Choi, Langmuir 33 (2017) 12398.
[79] F. Wang, R.J. Wong, J.H. Ho, Y. Jiang, R. Amal, ACS Appl. Mater. Interfaces 9 (2017) 30575.
[80] K. Awazu, M. Fujimaki, C. Rockstuhl, J. Tominaga, H. Murakami, Y. Ohki, N. Yoshida, T. Watanabe, J. Am. Chem. Soc. 130 (2008) 1676.
[81] H.A. Atwater, A. Polman, Nature Mater. 9 (2010) 205.
[82] Y. Ide, M. Matsuoka, M. Ogawa, J. Am. Chem. Soc. 132 (2010) 16762.
[83] M. Murdoch, G. Waterhouse, M. Nadeem, J. Metson, M. Keane, R. Howe, J. Llorca, H. Idriss, Nat. Chem. 3 (2011) 489.
[84] S.D. Standridge, G.C. Schatz, J.T. Hupp, J. Am. Chem. Soc. 131 (2009) 8407.
[85] R.-A. Doong, C.-H. Chen, R. Maithreepala, S.-M. Chang, Water Res. 35 (2001) 2873.
[86] M.G. Kang, H.-E. Han, K.-J. Kim, J. Photochem. Photobiol. A: Chem. 125 (1999) 119.
[87] X.F. Qu, J.J. Yuan, X.D. Deng, Y.C. Hou, Y.F. Wang, H.B. Song, Efficient Method to Form TiO2/CdS Nanotube Arrays Using Anodic Aluminum Oxide (AAO) Templates, Trans Tech Publ, 2017 p. 374.
[88] I. Tamiolakis, I.N. Lykakis, G.S. Armatas, Catal. Today 250 (2015) 180.
[89] S. Yin, H. Yamaki, M. Komatsu, Q. Zhang, J. Wang, Q. Tang, F. Saito, T. Sato, J. Mater. Chem. 13 (2003) 299.
[90] L. Zhang, W. Yu, C. Han, J. Guo, Q. Zhang, H. Xie, Q. Shao, Z. Sun, Z. Guo, J. Electrochem. Soc. 164 (2017) H651.
[91] Y. Xu, C.H. Langford, Langmuir 17 (2001) 897.
[92] A.K. Chandiran, S.M. Zakeeruddin, R. Humphry-, Baker, M.K. Nazeeruddin, M. Grätzel, F. Sauvage, ChemPhysChem 18 (2017) 2724.
[93] J. Hua, S.M. Zakeeruddin, J.-E. Moser, M. Grätzel, A. Hagfeldt, (2017).
[94] T.T. Pham, N. Mathews, Y.-M. Lam, S. Mhaisalkar, J. Electron. Mater. 46 (2017) 3801.
[95] B. O'regan, M. Grfitzeli, Nature 353 (1991) 737.
[96] Z.-C. Bi, H.T. Tien, Int. J. Hydrogen Energy 9 (1984) 717.
[97] B. Burfeindt, T. Hannappel, W. Storck, F. Willig, J. Phys. Chem. 100 (1996) 16463.
[98] T. Hannappel, B. Burfeindt, W. Storck, F. Willig, J. Phys. Chem. B 101 (1997) 6799.
[99] D. Pei, J. Luan, Int. J. Photoenergy 2012 (2012).
[100] S.G. Yan, J.T. Hupp, J. Phys. Chem. 100 (1996) 6867.
[101] R. Abe, K. Sayama, H. Arakawa, Chem. Phys. Lett. 362 (2002) 441.
[102] S. Ye, R. Wang, M.-Z. Wu, Y.-P. Yuan, Appl. Surface Sci. 358 (2015) 15.
[103] H.-Y. Chen, L.-G. Qiu, J.-D. Xiao, S. Ye, X. Jiang, Y.-P. Yuan, RSC Adv. 4 (2014) 22491.
[104] Y. Zhang, A. Thomas, M. Antonietti, X. Wang, J. Am. Chem. Soc. 131 (2008) 50.
[105] H. Ou, L. Lin, Y. Zheng, P. Yang, Y. Fang, X. Wang, Adv. Mater. 29 (2017) n/a-n/a.
[106] F. Dong, L. Wu, Y. Sun, M. Fu, Z. Wu, S. Lee, J. Mater. Chem. 21 (2011) 15171.
[107] H. Ou, P. Yang, L. Lin, M. Anpo, X. Wang, Angew. Chem. Int. Ed. 56 (2017) 10905.
[108] J. Zhang, J. Sun, K. Maeda, K. Domen, P. Liu, M. Antonietti, X. Fu, X. Wang, Energy Environ. Sci. 4 (2011) 675.
[109] L. Ci, L. Song, C. Jin, D. Jariwala, D. Wu, Y. Li, A. Srivastava, Z. Wang, K. Storr, L. Balicas, Nature Mater. 9 (2010) 430.
[110] J. Lu, K. Zhang, X.F. Liu, H. Zhang, T.C. Sum, A.H.C. Neto, K.P. Loh, Nat. Commun. 4 (2013) 2681.
[111] M. Zhang, Z. Luo, M. Zhou, C. Huang, X. Wang, Sci. China Mater. 58 (2015) 867.
[112] H. Yuan, X. Liu, F. Afshinmanesh, W. Li, G. Xu, J. Sun, B. Lian, A.G. Curto, G. Ye, Y. Hikita, Nat. Nanotech. 10 (2015) 707.
[113] J.R. Swierk, T.E. Mallouk, Chem. Soc. Rev. 42 (2013) 2357.
[114] K. Kalyanasundaram, M. Grätzel, Coord. Chem. Rev. 177 (1998) 347.
[115] S. Ardo, G.J. Meyer, Chem. Soc. Rev. 38 (2009) 115.
[116] W.M. Campbell, A.K. Burrell, D.L. Officer, K.W. Jolley, Coord. Chem. Rev. 248 (2004) 1363.
[117] A. Mishra, M.K. Fischer, P. Bäuerle, Angew. Chem. Int. Ed. 48 (2009) 2474.
[118] K. Kalyanasundaram, M. Gratzel, Angew. Chem. 91 (1979) 759.
[119] J.S. de Sourza, L.O.M. de Andrade, A.V. Müller, A.S. Polo, Nanomaterials for solar energy conversion: dye-sensitized solar cells based on ruthenium (II) Tris-heteroleptic compounds or natural dyes, Springer, 2018 p. 69.
[120] D. Morimoto, H. Yoshida, K. Sato, K. Saito, M. Yagi, S. Takagi, T. Yui, Langmuir 33 (2017) 3680.
[121] H.D. Abruna, A.Y. Teng, G.J. Samuels, T.J. Meyer, J. Am. Chem. Soc. 101 (1979) 6745.
[122] W.J. Youngblood, S.-H.A. Lee, Y. Kobayashi, E.A. Hernandez-Pagan, P.G. Hoertz, T.A. Moore, A.L. Moore, D. Gust, T.E. Mallouk, J. Am. Chem. Soc. 131 (2009) 926.
[123] F.E. Lytle, D.M. Hercules, J. Am. Chem. Soc. 91 (1969) 253.
[124] K. Kalyanasundaram, Photochemistry of Polypyridine and Porphyrin Complexes, Academic Press, 1991.
[125] N.H. Damrauer, G. Cerullo, A. Yeh, T.R. Boussie, C.V. Shank, J.K. McCusker, Science 275 (1997) 54.
[126] M.K. Nazeeruddin, A. Kay, I. Rodicio, R. Humphry-Baker, E. Müller, P. Liska, N. Vlachopoulos, M. Grätzel, J. Am. Chem. Soc. 115 (1993) 6382.
[127] P.A. Christensen, A. Harriman, G. Porter, P. Neta, J. Chem. Soc., Faraday Trans. 2 80 (1984) 1451.
[128] M.S. Eberhart, D. Wang, R.N. Sampaio, S.L. Marquard, B. Shan, M.K. Brennaman, G.J. Meyer, C. Dares, T.J. Meyer, J. Am. Chem. Soc. 139 (2017) 16248.
[129] A. Harriman, G.S. Nahor, S. Mosseri, P. Neta, J. Chem. Soc., Faraday Trans. 1 F 84 (1988) 2821.
[130] C.F. Negre, R.L. Milot, L.A. Martini, W. Ding, R.H. Crabtree, C.A. Schmuttenmaer, V.S. Batista, J. Phys. Chem. C 117 (2013) 24462.
[131] B.L. Watson, T.A. Moore, A.L. Moore, D. Gust, Dyes Pigm. 136 (2017) 893.
[132] S.H. Kang, M.J. Jeong, Y.K. Eom, I.T. Choi, S.M. Kwon, Y. Yoo, J. Kim, J. Kwon, J.H. Park, H.K. Kim, Adv. Energy Mater. 7 (2017).
[133] A. Kay, M. Graetzel, J. Phys. Chem. 97 (1993) 6272.
[134] T.M. Viseu, G. Hungerford, M.I.C. Ferreira, J. Phys. Chem. B 106 (2002) 1853.
[135] N. Robertson, Angew. Chem. Int. Ed. 45 (2006) 2338.
[136] Z. Shen, X. Zhang, F. Giordano, Y. Hu, J. Hua, S.M. Zakeeruddin, H. Tian, M. Grätzel, Mater. Chem. Front. 1 (2017) 181.
[137] M. Peng, B. Dong, X. Cai, W. Wang, X. Jiang, Y. Wang, Y. Yang, D. Zou, Solar Energy 150 (2017) 161.
[138] A. Hagfeldt, G. Boschloo, L. Sun, L. Kloo, H. Pettersson, Chem. Rev. 110 (2010) 6595.
[139] Y. Ooyama, Y. Harima, Eur. J. Org. Chem. 2009 (2009) 2903.
[140] K.-F. Chen, Y.-C. Hsu, Q. Wu, M.-C.P. Yeh, S.-S. Sun, Org. Lett. 11 (2008) 377.
[141] P. Qin, H. Zhu, T. Edvinsson, G. Boschloo, A. Hagfeldt, L. Sun, J. Am. Chem. Soc. 130 (2008) 8570.
[142] S. Ito, S.M. Zakeeruddin, R. Humphry-, Baker, P. Liska, R. Charvet, P. Comte, M. K. Nazeeruddin, P. Péchy, M. Takata, H. Miura, Adv. Mater. 18 (2006) 1202.

[143] S. Ito, H. Miura, S. Uchida, M. Takata, K. Sumioka, P. Liska, P. Comte, P. Péchy, M. Grätzel, Chem. Comm. (2008) 5194.
[144] K. Hara, Y. Dan-oh, C. Kasada, Y. Ohga, A. Shinpo, S. Suga, K. Sayama, H. Arakawa, Langmuir 20 (2004) 4205.
[145] T.-Y. Wu, M.-H. Tsao, F.-L. Chen, S.-G. Su, C.-W. Chang, H.-P. Wang, Y.-C. Lin, W.-C. Ou-Yang, I.-W. Sun, Int. J. Mol. Sci. 11 (2010) 329.
[146] Z.-S. Wang, K. Hara, Y. Dan-oh, C. Kasada, A. Shinpo, S. Suga, H. Arakawa, H. Sugihara, J. Phys. Chem. B 109 (2005) 3907.
[147] A. Hagfeldt, M. Graetzel, Chem. Rev. 95 (1995) 49.
[148] M. Grätzel, J. Photochem. Photobiol. A: Chem. 164 (2004) 3.
[149] L. Zhang, J.M. Cole, ACS Appl. Mater. Interfaces 7 (2015) 3427.
[150] I. Gillaizeau-Gauthier, F. Odobel, M. Alebbi, R. Argazzi, E. Costa, C.A. Bignozzi, P. Qu, G.J. Meyer, Inorg. Chem. 40 (2001) 6073.
[151] P. Péchy, F.P. Rotzinger, M.K. Nazeeruddin, O. Kohle, S.M. Zakeeruddin, R. Humphry-Baker, M. Grätzel, J. Chem. Soc. Chem. Commun. (1995) 65.
[152] G. Guerrero, J.G. Alauzun, M. Granier, D. Laurencin, P.H. Mutin, Dalton Trans. 42 (2013) 12569.
[153] T.A. Heimer, S.T. D'Arcangelis, F. Farzad, J.M. Stipkala, G.J. Meyer, Inorg. Chem. 35 (1996) 5319.
[154] N.J. Cherepy, G.P. Smestad, M. Grätzel, J.Z. Zhang, J. Phys. Chem. B 101 (1997) 9342.
[155] J. Yang, P.J. Bremer, I.L. Lamont, A.J. McQuillan, Langmuir 22 (2006) 10109.
[156] W.R. McNamara, R.C. Snoeberger III, G. Li, C. Richter, L.J. Allen, R.L. Milot, C.A. Schmuttenmaer, R.H. Crabtree, G.W. Brudvig, V.S. Batista, Energy Environ. Sci. 2 (2009) 1173.
[157] B.-K. An, W. Hu, P.L. Burn, P. Meredith, J. Phys. Chem. C 114 (2010) 17964.
[158] C. Beadle, S. Long, Biomass 8 (1985) 119.
[159] N. Nelson, C.F. Yocum, Annu. Rev. Plant Biol. 57 (2006) 521.
[160] Y. Umena, K. Kawakami, J.-R. Shen, N. Kamiya, Nature 473 (2011) 55.
[161] K.N. Ferreira, T.M. Iverson, K. Maghlaoui, J. Barber, S. Iwata, Science 303 (2004) 1831.
[162] E.S. Andreiadis, M. Chavarot-, Kerlidou, M. Fontecave, V. Artero, Photochem. Photobiol. 87 (2011) 946.
[163] R.J. Debus, B.A. Barry, G.T. Babcock, L. McIntosh, Proc. Natl. Acad. Sci. 85 (1988) 427.
[164] J. Pan, Y. Xu, G. Benkö, Y. Feyziyev, S. Styring, L. Sun, B. Åkermark, T. Polívka, V. Sundström, J. Phys. Chem. B 108 (2004) 12904.
[165] O. Johansson, H. Wolpher, M. Borgström, L. Hammarström, J. Bergquist, L. Sun, B. Åkermark, Chem. Comm. (2004) 194.
[166] T.A. Moore, D. Gust, P. Mathis, J.-C. Mialocq, C. Chachaty, R.V. Bensasson, E.J. Land, D. Doizi, P.A. Liddell, W.R. Lehman, Nature 307 (1984) 630.
[167] J.M. Sumliner, H. Lv, J. Fielden, Y.V. Geletii, C.L. Hill, Eur. J. Inorg. Chem. 2014 (2014) 635.
[168] C.H. van Oversteeg, H.Q. Doan, F.M. de Groot, T. Cuk, Chem. Soc. Rev. 46 (2017) 102.
[169] S. Hammes-Schiffer, Chem. Rev. 110 (2010) 6937.
[170] R.I. Cukier, D.G. Nocera, Annu. Rev. Phys. Chem. 49 (1998) 337.
[171] P. Du, R. Eisenberg, Energy Environ. Sci. 5 (2012) 6012.
[172] H. Lv, Y.V. Geletii, C. Zhao, J.W. Vickers, G. Zhu, Z. Luo, J. Song, T. Lian, D.G. Musaev, C.L. Hill, Chem. Soc. Rev. 41 (2012) 7572.
[173] Z. Huang, Z. Luo, Y.V. Geletii, J.W. Vickers, Q. Yin, D. Wu, Y. Hou, Y. Ding, J. Song, D.G. Musaev, J. Am. Chem. Soc. 133 (2011) 2068.
[174] A. Llobet, Molecular Water Oxidation Catalysis, John Wiley & Sons, 2014.
[175] W. Rüttinger, G.C. Dismukes, Chem. Rev. 97 (1997) 1.
[176] R. Brimblecombe, G.C. Dismukes, G.F. Swiegers, L. Spiccia, Dalton Trans. (2009) 9374.
[177] S.W. Gersten, G.J. Samuels, T.J. Meyer, J. Am. Chem. Soc. 104 (1982) 4029.
[178] N.D. McDaniel, F.J. Coughlin, L.L. Tinker, S. Bernhard, J. Am. Chem. Soc. 130 (2008) 210.
[179] E.N. Glass, J. Fielden, A.L. Kaledin, D.G. Musaev, T. Lian, C.L. Hill, Chem. A Eur. J. 20 (2014) 4297.
[180] J. Galan-Mascaros, 2017.
[181] J. Soriano-López, D.G. Musaev, C.L. Hill, J.R. Galán-Mascarós, J.J. Carbó, J.M. Poblet, J. Catal. 350 (2017) 56.
[182] S.M. Lauinger, B.D. Piercy, W. Li, Q. Yin, D.L. Collins-Wildman, E.N. Glass, M.D. Losego, D. Wang, Y.V. Geletii, C.L. Hill, ACS Appl. Mater. Interfaces 9 (2017) 35048.
[183] G. Zhu, Y.V. Geletii, P. Kögerler, H. Schilder, J. Song, S. Lense, C. Zhao, K.I. Hardcastle, D.G. Musaev, C.L. Hill, Dalton Trans. 41 (2012) 2084.
[184] D.L. Long, R. Tsunashima, L. Cronin, Angew. Chem. Int. Ed. 49 (2010) 1736.
[185] V.W. Day, W. Klemperer, Science 228 (1985) 533.
[186] M. Pope, A. Muller, J.J. Borrás-Almenar, (2003) 3–31.
[187] A. Sartorel, M. Carraro, G. Scorrano, R.D. Zorzi, S. Geremia, N.D. McDaniel, S. Bernhard, M. Bonchio, J. Am. Chem. Soc. 130 (2008) 5006.
[188] Y.V. Geletii, B. Botar, P. Kögerler, D.A. Hillesheim, D.G. Musaev, C.L. Hill, Angew. Chem. 120 (2008) 3960.
[189] M. Schilling, F.H. Hodel, S. Luber, ChemSusChem 10 (2017) 4561.
[190] C.N. Brodsky, R.G. Hadt, D. Hayes, B.J. Reinhart, N. Li, L.X. Chen, D.G. Nocera, Proc. Natl. Acad. Sci. 114 (2017) 3855.
[191] S. Berardi, G. La Ganga, M. Natali, I. Bazzan, F. Puntoriero, A. Sartorel, F. Scandola, S. Campagna, M. Bonchio, J. Am. Chem. Soc. 134 (2012) 11104.
[192] N.S. McCool, D.M. Robinson, J.E. Sheats, G.C. Dismukes, J. Am. Chem. Soc. 133 (2011) 11446.
[193] J. Kiwi, M. Grätzel, Angew. Chem. Int. Ed. 18 (1979) 624.
[194] J. Barber, Chem. Soc. Rev. 38 (2009) 185.
[195] H. Dau, M. Haumann, Coord. Chem. Rev. 252 (2008) 273.
[196] H. Dau, C. Limberg, T. Reier, M. Risch, S. Roggan, P. Strasser, ChemCatChem 2 (2010) 724.
[197] K. Sauer, Acc. Chem. Rev. 13 (1980) 249.
[198] T.C. Wen, C.C. Hu, J. Electrochem. Soc. 139 (1992) 2158.
[199] A. Harriman, I.J. Pickering, J.M. Thomas, P.A. Christensen, J. Chem. Soc., Faraday Trans. 1 F 84 (1988) 2795.
[200] G. Nahor, P. Neta, P. Hambright, A. Thompson Jr., A. Harriman, J. Phys. Chem. 93 (1989) 6181.
[201] Y. Lee, J. Suntivich, K.J. May, E.E. Perry, Y. Shao-Horn, J. Phys. Chem. Lett. 3 (2012) 399.
[202] A. Harriman, M.-C. Richoux, P.A. Christensen, S. Mosseri, P. Neta, J. Chem. Soc., Faraday Trans. 1 F 83 (1987) 3001.
[203] J. Kiwi, M. Grätzel, Angew. Chem. Int. Ed. 18 (1979) 624.
[204] Y. Kim, P.K. Dutta, J. Phys. Chem. C 111 (2007) 10575.
[205] D. Gust, T.A. Moore, A.L. Moore, Acc. Chem. Rev. 42 (2009) 1890.
[206] Y. Zhao, J.R. Swierk, J.D. Megiatto, B. Sherman, W.J. Youngblood, D. Qin, D.M. Lentz, A.L. Moore, T.A. Moore, D. Gust, Proc. Natl. Acad. Sci. 109 (2012) 15612.
[207] P. Faller, C. Goussias, A.W. Rutherford, S. Un, Proc. Natl. Acad. Sci. 100 (2003) 8732.
[208] J. Stubbe, D.G. Nocera, C.S. Yee, M.C. Chang, Chem. Rev. 103 (2003) 2167.
[209] L. Trotochaud, T.J. Mills, S.W. Boettcher, J. Phys. Chem. Lett. 4 (2013) 931.
[210] F.E. Osterloh, B.A. Parkinson, MRS Bull. 36 (2011) 17.
[211] E. Reisner, D.J. Powell, C. Cavazza, J.C. Fontecilla-Camps, F.A. Armstrong, J. Am. Chem. Soc. 131 (2009) 18457.
[212] M. Hambourger, M. Gervaldo, D. Svedruzic, P.W. King, D. Gust, M. Ghirardi, A. L. Moore, T.A. Moore, J. Am. Chem. Soc. 130 (2008) 2015.
[213] M.M. Roubelakis, D.K. Bediako, D.K. Dogutan, D.G. Nocera, Energy Environ. Sci. 5 (2012) 7737.
[214] Z. Jin, X. Zhang, G. Lu, S. Li, J. Mol. Cat. A: Chem. 259 (2006) 275.
[215] Z. Jin, X. Zhang, Y. Li, S. Li, G. Lu, Catal. Commun. 8 (2007) 1267.
[216] Q. Li, L. Chen, G. Lu, J. Phys. Chem. C 111 (2007) 11494.
[217] Q. Li, Z. Jin, Z. Peng, Y. Li, S. Li, G. Lu, J. Phys. Chem. C 111 (2007) 8237.
[218] Y. Li, M. Guo, S. Peng, G. Lu, S. Li, Int. J. Hydrogen Energy 34 (2009) 5629.
[219] E. Bae, W. Choi, J. Phys. Chem. B 110 (2006) 14792.
[220] J. Lobedank, E. Bellmann, J.D. Bendig, J. Photochem. Photobiol. A: Chem. 108 (1997) 89.
[221] S.T. Cheung, A.K. Fung, M.H. Lam, Chemosphere 36 (1998) 2461.
[222] A.K. Fung, B.K. Chiu, M.H. Lam, Water Res. 37 (2003) 1939.
[223] S. Min, F. Wang, Y. Han, J. Mat. Sci. 42 (2007) 9966.
[224] L. Song, R. Qiu, Y. Mo, D. Zhang, H. Wei, Y. Xiong, Catal. Commun. 8 (2007) 429.
[225] A. Bard, J. Photochem. 10 (1979) 59.
[226] K. Domen, S. Naito, M. Soma, T. Onishi, K. Tamaru, J. Chem, Soc. Chem. Commun. (1980) 543.
[227] T. Kawai, T. Sakata, Chem. Phys. Lett. 72 (1980) 87.
[228] A. Kudo, J. Catal. 111 (1988) 67.
[229] Y. Inoue, T. Niiyama, Y. Asai, K. Sato, J. Chem. Soc. Chem. Commun. 1992 (1992) 579.
[230] R. Konta, T. Ishii, H. Kato, A. Kudo, J. Phys. Chem. B 108 (2004) 8992.
[231] A. Kudo, Int. J. Hydrogen Energy 32 (2007) 2673.
[232] K. Ikarashi, J. Phys. Chem. B 106 (2002) 9048.
[233] J. Sato, N. Saito, H. Nishiyama, Y. Inoue, J. Phys. Chem. B 105 (2001) 6061.
[234] Y. Inoue, Energy Environ. Sci. 2 (2009) 364.
[235] R. Abe, K. Sayama, K. Domen, H. Arakawa, Chem. Phys. Lett. 344 (2001) 339.
[236] K. Sayama, K. Mukasa, R. Abe, Y. Abe, H. Arakawa, Chem. Commun. (2001) 2416.
[237] K. Maeda, K. Domen, J. Phys. Chem. C 111 (2007) 7851.
[238] A. Ishikawa, J. Am. Chem. Soc. 124 (2002) 13547.
[239] G. Hitoki, Chem. Lett. 7 (2002) 736.
[240] J. Sato, J. Am. Chem. Soc. 127 (2005) 4150.
[241] K. Maeda, J. Am. Chem. Soc. 127 (2005) 8286.
[242] Y. Sasaki, H. Nemoto, K. Saito, A. Kudo, J. Phys. Chem. C 113 (2009) 17536.
[243] K. Maeda, Chem. Commun. 49 (2013) 8404.
[244] R. Asai, Chem. Commun. 50 (2014) 2543.
[245] Y. Qi, Chem. Sci. 8 (2017) 437.
[246] C. Pan, Angew. Chem. Int. Ed. 54 (2015) 2955.
[247] C. Pan, J. Mater Chem A 4 (2016) 4544.
[248] G. Zhang, Z. Lan, L. Lin, S. Lin, X. Wang, Chem. Sci. 7 (2016) 3062.
[249] F. Bozoglian, S. Romain, M.Z. Ertem, T.K. Todorova, C. Sens, J. Mola, M. Rodriguez, I. Romero, J. Benet-Buchholz, X. Fontrodona, J. Am. Chem. Soc. 131 (2009) 15176.
[250] Z. Deng, H.-W. Tseng, R. Zong, D. Wang, R. Thummel, Inorg. Chem. 47 (2008) 1835.
[251] Y. Xu, T.R. Åkermark, V. Gyollai, D. Zou, L. Eriksson, L. Duan, R. Zhang, B.R. Åkermark, L. Sun, Inorg. Chem. 48 (2009) 2717.
[252] Y. Xu, A. Fischer, L. Duan, L. Tong, E. Gabrielsson, B. Åkermark, L. Sun, Angew. Chem. Int. Ed. 49 (2010) 8934.
[253] F. Liu, T. Cardolaccia, B.J. Hornstein, J.R. Schoonover, T.J. Meyer, J. Am. Chem. Soc. 129 (2007) 2446.
[254] T. Wada, K. Tsuge, K. Tanaka, Inorg. Chem. 40 (2001) 329.
[255] R. Zong, R.P. Thummel, J. Am. Chem. Soc. 127 (2005) 12802.
[256] J.J. Concepcion, J.W. Jurss, J.L. Templeton, T.J. Meyer, J. Am. Chem. Soc. 130 (2008) 16462.
[257] J.J. Concepcion, J.W. Jurss, M.R. Norris, Z. Chen, J.L. Templeton, T.J. Meyer, Inorg. Chem. 49 (2010) 1277.
[258] Y.V. Geletii, Z. Huang, Y. Hou, D.G. Musaev, T. Lian, C.L. Hill, J. Am. Chem. Soc. 131 (2009) 7522.

[259] C. Besson, Z. Huang, Y.V. Geletii, S. Lense, K.I. Hardcastle, D.G. Musaev, T. Lian, A. Proust, C.L. Hill, Chem. Comm. 46 (2010) 2784.
[260] R. Cao, H. Ma, Y.V. Geletii, K.I. Hardcastle, C.L. Hill, Inorg. Chem. 48 (2009) 5596.
[261] M. Murakami, D. Hong, T. Suenobu, S. Yamaguchi, T. Ogura, S. Fukuzumi, J. Am. Chem. Soc. 133 (2011) 11605.
[262] S. Tanaka, M. Annaka, K. Sakai, Chem. Comm. 48 (2012) 1653.
[263] R. Brimblecombe, D.R. Kolling, A.M. Bond, G.C. Dismukes, G.F. Swiegers, L. Spiccia, Inorg. Chem. 48 (2009) 7269.
[264] A. Harriman, G. Porter, P. Walters, J. Chem. Soc., Faraday Trans. 2 77 (1981) 2373.
[265] M. Hara, C.C. Waraksa, J.T. Lean, B.A. Lewis, T.E. Mallouk, J. Phys. Chem. A 104 (2000) 5275.
[266] P.G. Hoertz, Y.-I. Kim, W.J. Youngblood, T.E. Mallouk, J. Phys. Chem. B 111 (2007) 6845.
[267] Y. Zhao, E.A. Hernandez-Pagan, N.M. Vargas-Barbosa, J.L. Dysart, T.E. Mallouk, J. Phys. Chem. Lett. 2 (2011) 402.
[268] F. Jiao, H. Frei, Angew. Chem. 121 (2009) 1873.
[269] B.P. Uberuaga, X.-M. Bai, J. Phys. Condens. Matter 23 (2011) 435004.
[270] R. Kaur, B. Pal, New J. Chem. 39 (2015) 5966.
[271] H. Wang, L. Zhang, Z. Chen, J. Hu, S. Li, Z. Wang, J. Liu, X. Wang, Chem. Soc. Rev. 43 (2014) 5234.